1

Introduction to 4D Printing: Concepts and Material Systems

Xiao Kuang, Liang Yue, and H. Jerry Qi

Georgia Institute of Technology, The George W. Woodruff School of Mechanical Engineering, 801 Ferst Dr., Atlanta, GA 30332, USA

1.1 Background

In 2013, Tibbits introduced the concept of "four-dimensional printing" (or 4D printing) [1]. He used an inkjet printer to print active (or programmable) polymer composites, whose shape could evolve with time under the water. Soon after, Qi and coworkers presented the concept of printed active composites (PACs), which can shift into various complex configurations by leveraging shape-memory polymers (SMPs) [2]. These pioneering works open the new field of 4D printing, which attracts increasing attention in research communities and industry.

In Figure 1.1a, the schematic illustration shows the difference of structures from one-dimensional (1D) to 4D. The structures show improved complexity in dimensions from 1D to three-dimensional (3D). 4D printing is initially defined as "3D-printed shape + time," where the fourth dimension is time [2–6]. Currently, the definition of 4D printing has been broadened to include not only the shape but also the property and functionality of 3D-printed structures that would change with time under a predetermined stimulus after printing. In 4D printing technique, stimuli-responsive materials and proper structural design are usually used for 3D printing of shape-programmable structures. Compared with conventional 3D-printed static objects, 4D-printed structures are able to change their shape, size, color, or other functional properties with time under external stimuli. The on-demand shape and property changes after printing enable several prominent advantages. First, it allows the direct manufacturing of smart and intelligent structures/devices. Second, it saves printing time and materials, particularly, for thin-wall structure fabrication. Third, it can save storage and transportation space for printed parts [7]. Due to these reasons, 4D printing has become a fast-growing research field in various disciplines, such as smart materials and advanced manufacturing.

4D printing has witnessed significant progress during the past years, thanks to the tremendous advances in 3D printing techniques, stimuli-responsive materials, and design and modeling-based methods [3, 8–11]. 3D printing, or additive manufacturing (AM), becomes a disruptive technology for advanced manufacturing [12, 13].

Additive Manufacturing Technology: Design, Optimization, and Modeling, First Edition. Edited by Kun Zhou.

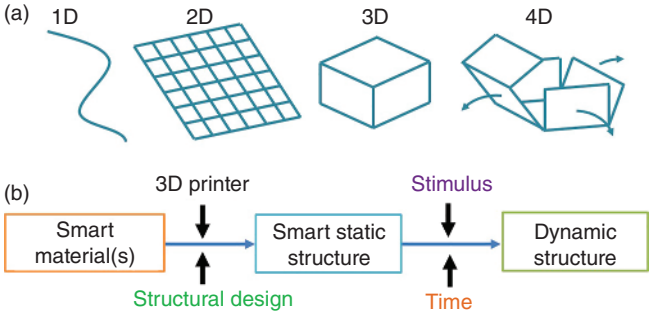

Figure 1.1 (a) Schematic illustration of 1D to 4D. (b) Flowchart showing the basic elements of 4D printing. Source: Momeni et al. [3]/with permission of Elsevier.

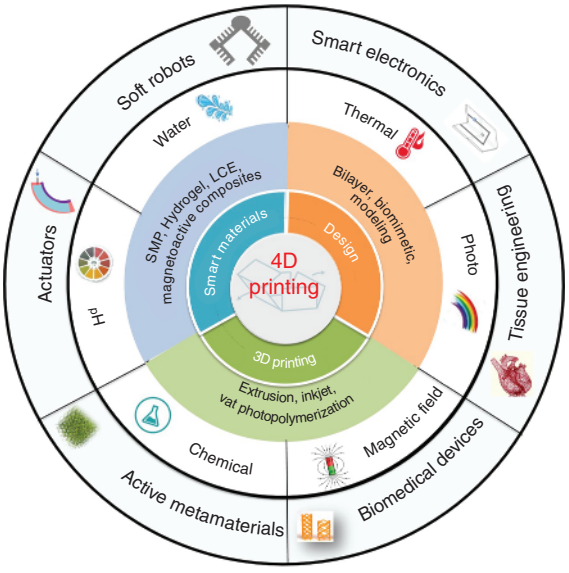

Figure 1.2 Schematic summary of the primary 3D printing techniques, various shape-programmable materials, and commonly used design approaches for 4D printing and their applications.

According to predetermined design models (such as computer-aided design [CAD]), raw materials in various forms (powder, filament, or liquid) can be deposited by different printing modalities, such as extrusion-based printing, inkjet-based printing, and vat photopolymerization-based printing (Figure 1.2). Notably, multi-material 3D printing by constructing heterogeneous structures with spatial control of material distributions becomes a leading direction for 4D printing. Metals [14], ceramics [15, 16], and polymers [2, 4, 17] have been used for 4D printing. However, polymers are still the primary materials for 4D printing due to their cost-effectiveness, diverse stimuli-responding, and large deformability [14]. For example, shape-programmable polymers can be engineered to respond to a wide range of physical and/or chemical stimuli, such as temperature, chemical, light, and magnetic field. The most extensively studied shape-programmable smart polymers for 4D printing include SMPs, hydrogels, liquid crystal elastomers (LCEs), and magnetoactive soft materials (MSMs). The 4D-printed structures with

on-demand complex geometry and stimuli-responsive capability find applications in various fields, including actuators, soft robots, active metamaterials, smart electronics, self-folding structures, biomedical devices, and tissue engineering [18–24]. The shape-shifting performance of 4D-printed structures is highly dependent on both the properties of shape-programmable materials and structures. Several review papers in 4D printing can be found with different focuses on stimuli-responsive materials [7, 25, 26], shape-changing mechanisms [3, 27, 28], and applications [18, 29]. This chapter provides a fundamental understanding and recent advances in programmable polymeric material systems for 4D printing. It is organized by starting with an overview of 3D printing techniques, followed by the advances in smart material systems for 4D printing. Particular attention is paid to the use of the single-material and multi-material design of smart materials with different shape-changing mechanisms for shape-changing. In addition, we briefly introduce the modeling-guided design for 4D printing to predict the shape-shifting. To close, we discuss the major challenges and perspectives in 4D printing.

1.2 Overview of 3D Printing Techniques

According to International Organization for Standardization (ISO Technical Committee 261) and American Society for Testing and Materials (ASTM) International (Committee F42), AM technologies are classified into seven groups, including binder jetting, directed energy deposition, material extrusion, material jetting, powder bed fusion, sheet lamination, and vat photopolymerization [30]. In the following section, we introduce the 3D printing methods for polymers and composites most relevant to 4D printing. In most cases, 3D printers are only compatible with single-material processing, meaning a single material is printed by one printing technique in one printing job. By contrast, multi-material 3D printers have been developed to fabricate heterogeneous structures with precisely controlled materials distribution to manipulate more complex shape evolution and pathway.

1.2.1 Single-Material 3D Printing Techniques

Extrusion-based printing, inkjet printing, and vat photopolymerization-based printing are extensively used 3D printing techniques for 4D printing (Figure 1.3). Among them, the most versatile printing technique is extrusion-based printing, which constructs the 3D object in a line-by-line and then a layer-by-layer manner. Depending on the ink, extrusion-based printing is divided into fused filament fabrication (FFF) (or fused deposition modeling [FDM]) and direct-ink-writing (DIW). In the FFF process, a solid filament is fed into a heating nozzle to form a polymer melt, which is continuously deposited onto a building tray with a controlled temperature and then solidified by environmental cooling. For example, engineering thermoplastics and composites, such as acrylonitrile butadiene styrene (ABS), polylactic acid (PLA), polyurethane (PU), as well as fiber or particle-embedded

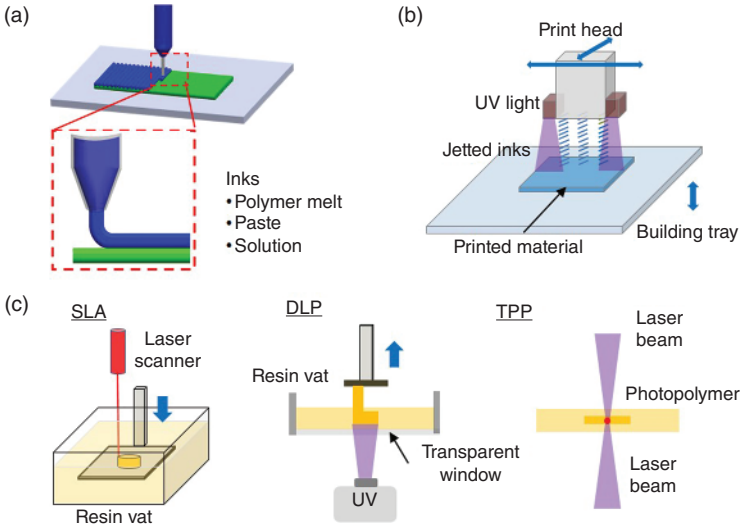

Figure 1.3 Schematics of three major 3D printing techniques for polymers: extrusion-based printing, inkjet-based printing, and vat photopolymerization-based printing. Source: Kuang [31]/with permission of Elsevier.

composites, can be printed by FFF [32]. In FFF, residual stress usually exists due to the shearing and moving nozzle's temperature gradient and polymer chain alignment [33, 34]. This residual stress can be utilized to induce shape-shifting by stress releasing after printing [35, 36]. For FFF-based 4D printing, the shape memory effect (SME) of printed plastics is also frequently used to accommodate shape change [37]. By contrast, DIW uses a mechanical extruder or pressure to deposit paste or solution ink, solidified later by solvent evaporation, UV curing, or thermal curing. The prominent advantage of extrusion-based methods is their applicability to a broad width of inks with different curing chemistry and viscosity. Assisted by post-curing, DIW has been used to print different engineering thermosetting polymers [38–42], and functional materials, such as MSMs [43–47] and LCEs [48–53]. Compared with FFF printing with weak interfaces between filaments [54], DIW-printed materials with post-curing generally present a strong interface. The resolution of FFF and DIW is typically in the range of 100–200 μm, limited by the nozzle diameter. In addition, the extrusion-based methods usually show a low printing speed due to the line-by-line fabrication manner.

Inkjet 3D printing is another popular method for photopolymer printing. During inkjet printing, photocurable ink drops (in the size of 20–40 μm) are deposited onto the building bed from printing nozzles controlled by the piezoelectric device, heating modules, or electromagnetic unit, followed by UV curing to form a solid layer [55]. The process is repeated until the whole structure is built. Various photocurable acrylate-based monomers and crosslinkers are formulated as low-viscosity inks to print materials with different properties [56]. Inkjet printing has high resolution with a typical in-plane resolution of 30–40 μm [57]. Usually, a support material made of weak and water-soluble polymer is used to allow complex

structure printing. Despite its many advantages, inkjet printing suffers from the high equipment cost and the stringent requirement on ink viscosity [58].

Vat photopolymerization-based printing is a fast-growing method for 3D printing polymers. This printing technique includes several different printing modalities, including stereolithography (SLA), digital light processing (DLP), and two-photon polymerization (TPP), which relies on the light to selectively cure photo-sensitive polymer resins to build 3D structures. SLA is the earliest 3D printing method, which employs a UV laser beam to rapidly solidify the photopolymers inks [56, 57]. However, the line-by-line scanning-based SLA printing is usually slow, especially in large part. By contrast, DLP exploits dynamic light patterns by digital micromirror devices (DMDs) to cure a layer of resin at a time, enabling fast printing [59]. The emergence of continuous liquid interface production (CLIP) is a breakthrough for DLP, which further enhances the printing speed and is among the fastest 3D printing technology suitable for large-scale industrial production [60, 61]. CLIP uses an oxygen-permeable film to form a dead zone between the transparent window and liquid, allowing continuous build stage elevation without ink renewal step. The in-plane resolution of DLP falls in the range of 50–100 μm, determined by the DMDs and focusing lens used in the projector. By coupling a proper lens system with a DLP projector, micro-DLP (μDLP; or projection micro-stereolithography, PμSLA) has been developed to realize higher resolution up to 0.6 μm [59, 62]. Nanoscale printing resolution is achieved by using TPP-based printing. The simultaneous absorption of two photons at the high-intensity focal point of two lasers allows printing structures with a submicron resolution typically around 40–100 nm [63].

1.2.2 Multi-Material 3D Printing

Driven by the need to fabricate heterogeneous functional structures and devices, multi-material 3D printing has been developed and attracted great attention [64–69]. The direct approach to multi-material printing uses multiple nozzle extruders [67, 69–73]. Microfluidics-extrusion [74] and micromixer-based co-extruders [66, 75–77] have also been developed for extrusion-based multi-material printing. Espalin et al. [72] developed a multi-material FFF system to print parts either using discrete multi-materials or varying building processes. Recently, Lewis and coworkers developed a multi-material multi-nozzle DIW printing approach to realize high-resolution, high-speed multi-material printing [67]. Besides, multi-material DIW printing was achieved using photothermal dual-cure resins [78].

The PolyJet technology by Stratasys enables inkjet printing of digital materials and multi-materials using multiple print heads and inks [56]. To achieve this, multiple inks were deposited in a predetermined ratio and cured together, generating so-called digital materials with digitalized mechanical properties within a certain range. This technique allows for the facile fabrication of parts composed of materials with widely tunable mechanical and thermomechanical properties [56, 57]. However, the resolution of multi-material printing by PolyJet printer is reduced to 200–400 μm [79].

Multi-material printing can be achieved by switchable multiple resin vats [80–82]. Wicker and coworker [80] utilized the scanning SLA system with multiple vat carousel designs to print 3D multi-material objects. The process requires a cleaning step (in a cleaning vat) before being immersed in a different material vat to reduce contamination. Recently, Ge and coworkers developed multi-material PμSLA printing by switching between different ink droplets and using high-pressure air for surface cleaning [81, 82]. Instead of using multiple resin vats, single-vat DLP printing of multi-materials has been achieved by selective wavelength photocuring [83, 84], and grayscale printing [85, 86]. Particularly, grayscale DLP printing using grayscale images for spatially controlled light dose correlated with different crosslinking densities and mechanical properties. The monochromic images with grayscale red, green, and blue (RGB) values ranging from 255 to 0 (brightness from 1 to 0) indicate full light intensity to completely dark. By leveraging the material properties gradients by the grayscale DLP, various shape-shifting materials using different mechanisms can be created for 4D printing [87–89].

Besides, integrated multiple printing technologies (or hybridizing) can provide or improve spatial control of material, geometry, and functionality. Early in 2005, Wicker's group [90] integrated commercial SLA machines with DIW for automated and efficient hybrid manufacturing of complex electrical devices. Recently, Peng et al. [91] reported a hybrid printing system consisting of top-down DLP printing and DIW printing for multi-material 3D printing (Figure 1.4a). The DLP module enabled high-resolution, high-speed printing of geometrical complex structures using various photopolymer inks. The DIW printing module was used for printing functional materials, such as LCEs and conductive silver ink. With this technique, multi-material soft robots and actuators could be directly printed in one print job. Roach et al. [92] developed a multi-material multi-method (m4) AM platform by integrating four different printing modules (inkjet printing, FFF, DIW, and aerosol jetting), and robotic arms for pick-and-place (PnP), as well as intense pulsed light (IPL) sintering system (Figure 1.4b). With this platform, complex structures and functional devices, including actuators, soft robotics, and electronics, could be readily printed.

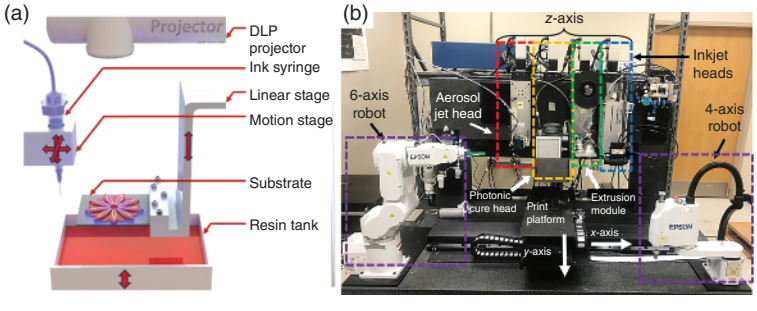

Figure 1.4 Typical examples of multi-material printing techniques. (a) Hybrid 3D printer integrating top-down DLP printing and DIW printing techniques. Source: Peng et al. [91]/with permission of Elsevier. (b) Picture of a multi-material multi-method 3D printing platform. Source: Roach et al. [92]/with permission of Elsevier B.V.

1.3 Shape-Programmable Materials for 4D Printing

Shape-programmable materials are widely used as stimuli-responsive materials for 4D printing. Four different types of shape-programmable materials, namely SMPs, hydrogels, LCEs, and MSMs and their composites, are extensively studied [93]. These materials have different shape-shifting mechanisms. SMPs are mechanically programmed in a temporary shape, which is triggered by external stimuli for shape recovery due to the entropic elasticity of the polymer network [94, 95]. Shape-changing of hydrogels originates from water uptake/release by swelling and shrinkage under external stimuli [96]. LCEs enable reversible shape change via the phase transition between the nematic (N) state and isotropic (I) state [97, 98]. MSMs composed of magnetic particles embedding soft polymer matrix can undergo rapid and reversible shape actuation, owing to the interactions between magnetic particles and magnetic fields [99, 100]. Although there are some other materials and shape-morphing mechanisms, such as polymerization-induced volume shrinkage [87], evaporation-induced shrinkage [101, 102], and thermal expansion mismatch [103], we will focus on using the aforementioned shape-programmable materials for 4D printing in this chapter. This section will summarize advances in these shape-programmable materials, and typical examples will be provided.

1.3.1 Shape-Memory Polymers and Composites

SMPs are smart materials showing the SME, which has been extensively used for 4D printing. For SMPs, temporary shapes can first be programmed, and then the initial shape can be recovered in response to external stimuli, such as heat [104–109], solvent [110–114], and light [115–118]. Vernon first discovered the SME in 1941, when he used e-beam or peroxide crosslinked high-density polyethylene to make heat-shrinkable tubes and films [119].

SME can be understood by the concept of "fixing phase" and "switching phase" [94, 95]. In the form of chemical or physical crosslinking points, the fixing phase can hold the permanent shape of the material. By contrast, the switching phase can be either phase level (amorphous and crystalline) or molecular level (supramolecular entities and reversible molecular units). The switching phase can transform between an active state and a frozen state featuring different chain mobility. The shape fixing and recovery of SMPs are realized by altering the chain mobility via applying and eliminating external stimuli. Heat is the most common trigger for SMPs, which can be achieved by direct heating or indirect heating [120]. Phase transition temperature (T_t), including glass transition temperature (T_g) and melting temperature (T_m), is employed by heating to trigger the shape change (or shape recovery) in SMPs. In thermally activated SMPs, the initial shape is in the thermodynamically stable conformation with the highest entropy. Chain mobility is significantly enhanced upon heating above T_t, allowing for deformation under external force. The programmed shapes possess lower entropy. When SMPs are cooled down to a temperature lower than T_t and undergo the phase transition (glass transition or crystallization), a metastable state with relatively low energy is

obtained, leading to the temporary shape fixing of SMP. Upon reheating above T_t, SMPs regain high chain mobility for shape recovery driven by entropic elasticity.

1.3.1.1 Single SMP

Various semicrystalline polymers (such as PLA and PCL) [121, 122] and amorphous polymers (such as polyacrylate and epoxy) [123] with tunable thermomechanical properties have been used as thermally triggered SMPs, which are good candidates for [124] 4D printing. FFF can print physically crosslinked semicrystalline polymers for 4D printing, while chemically crosslinked amorphous SMPs with better shape memory performance are mainly printed via vat photopolymerization-based techniques using various photopolymer inks. The T_g and stretchability of polyacrylate-based photopolymers can be tuned by the rigidity of acrylate monomers and crosslinker content [124, 125]. For example, Ge et al. [68] used benzyl methacrylate (BMA) and different difunctional (meth)acrylates for high-resolution PμSL printing of SMPs with tunable mechanical and thermomechanical properties (Figure 1.5a). The rubbery modulus increased from 1 to 100 MPa by increasing the crosslinker content. In addition, by using crosslinkers with different chain rigidity, the T_g of the polymer was tuned from −50 to 180 °C. However, the aforementioned methacrylate-based resins required very high exposure energy (or light dose) to accommodate adequate curing due to slow crosslinking. Figure 1.5a also shows the shape recovery of 3D-printed Eiffel Tower model from a programmed bent shape.

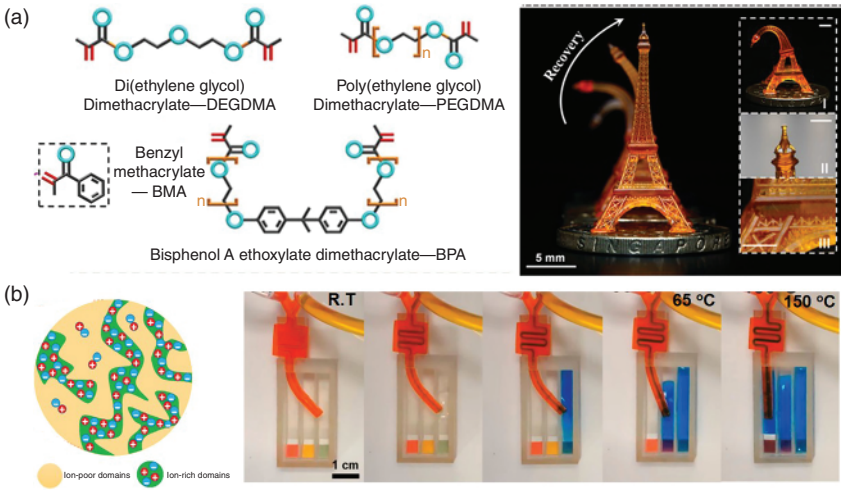

Figure 1.5 Design examples of SMP for 4D printing of SMP. (a) The chemical structures of a rigid mono-functional monomer of several and difunctional oligomers as crosslinkers for PμSL printing of SMPs. The printed high-resolution Eiffel Tower with shape memory effect. Source: Ge et al. [68]/with permission of Springer Nature. (b) A microphase separation SMP can be printed by DLP via photopolymerization-induced microphase separation. The use of the printed SMP with two different T_g for selective feeding process using triple SME devices. Source: Peng et al. [126]/with permission of American Chemical Society.

Multiple shape-shifting by multi-SME in single-material SMPs has also been achieved by 3D printing. For example, polymers with a broad phase transition temperature can realize multi-SME [127–129]. Yu et al. [130] used Objet Connex printer material library to print a digital material Gray 60 with a broad T_g (a range of ~40 °C) with multi-SME. The printed SMP was programmed into different temporary shapes at different temperatures to obtain sequential shape-changing. Recently, Peng et al. [126] reported the DLP printing of a microphase-separated material for a triple SME. An ion–pair comonomer was introduced and served as a physical crosslinker in ink. The photopolymerization-induced microphase separation could rapidly occur during printing, and two separated glass transition temperatures were obtained in the material. It was demonstrated that the printed microfluidic devices could be used as selective feeding devices using temperature-dependent shape-shifting (Figure 1.5b).

To enhance the properties of printed SMPs, inks can be rationally designed to modulate the material network architectures. To this end, the molecular engineering of interpenetrating polymer network (IPN) and semi-interpenetrating polymer network (semi-IPN) has been widely used. Kuang et al. [131] developed a new photopolymer ink containing aliphatic urethane diacrylate (AUD), *n*-butyl acrylate, and semicrystalline polycaprolactone (PCL) as well as fumed silica (rheology modifier) for UV-assisted DIW printing (Figure 1.6a). The composite ink was deposited at around 70 °C and then crosslinked by photocuring. The obtained semi-IPN polymer composite contains a percolating network of nanoscale crystals and a covalent network. The loosely crosslinked chemical

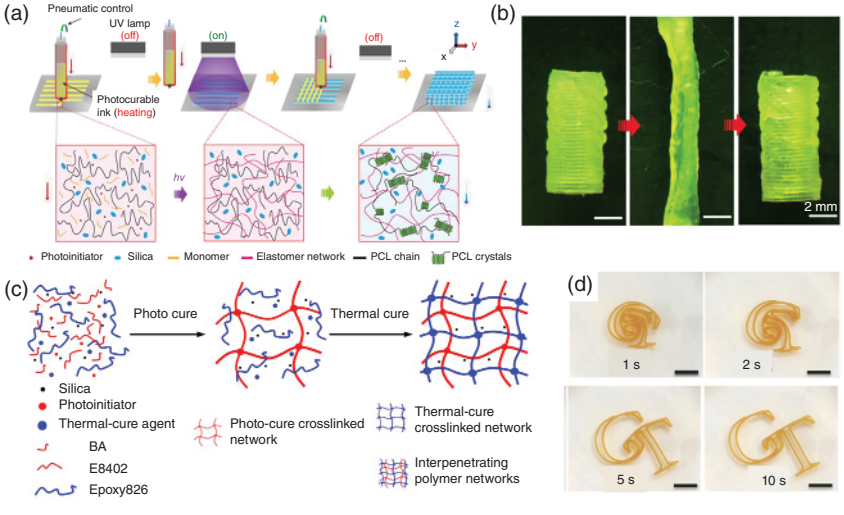

Figure 1.6 SMP composites with hybrid polymer network design. (a) Semi-interpenetrating polymer network SMP was printed by UV-assisted DIW printing [131]. (b) DIW-printed tubes with shape memory effect [131]. (c) Interpenetrating polymer network SMP was printed by DIW via a photothermal dual-cure approach [39]. (d) The results shape the recovery of printed epoxy SMP in a "GT" logo in an oil bath [39]. Source: (a) and (b) Kuang et al. [131]/with permission of American Chemical Society. (c) and (d) Chen et al. [39]/with permission of Royal Society of Chemistry.

network and PCL crystals acted as fixing and switching phases for the SME with large deformation, respectively. Besides, the PCL nanocrystals played the role of a healing agent for material self-healing. The SME could facilitate crack closing and assist the material healing process. It was shown shape memory tubular structures can be printed with on-demand size for vascular repair applications (Figure 1.6b). Zhang et al. [132] used DLP for high-resolution 4D printing using similar material systems. Similarly, PCL is incorporated into a methacrylate photopolymer ink for high-resolution (up to 30 μm) printing of SMPs.

IPN can be obtained by dual-curing or photothermal two-stage curing approaches. Yu et al. [133] reported the use of epoxy-acrylate hybrid photopolymer to print SMP via the SLA 3D printing technique. A polyacrylate-*co*-epoxy particle was first performed and dispersed in epoxy resin to enhance the toughness. Then, both free radical and cationic initiators are used to simultaneously cure the acrylates and epoxy resin by UV irradiation during printing. Finally, the printed SMP shows good thermal stability, high strength, and good toughness. To further enhance the mechanical properties, dual-stage curing was adopted to fabricate IPN [39, 134, 135]. Chen et al. [39] developed a hybrid ink containing photocurable acrylates and thermal-curable epoxy for UV-assisted DIW printing. The UV curing leads to a first polymer network in the green part, which is further treated with the second-stage (thermal-curing) to boost the mechanical properties (Figure 1.6c). The modulus and T_g of SMPs can be tuned by altering the ratio of the photocurable and thermal-curable components. With this approach, IPN-based SMPs with high toughness and high resolution can be printed (Figure 1.6d).

1.3.1.2 SMP Nanocomposites

Thermal activation of SMPs for shape change relies on thermal energy conduction for the material. As pure polymers usually possess low thermal conductivities, the shape recovery rate of large-size SMPs is usually low. To improve the shape recovery speed of SMPs, indirect heating methods have been explored. This can be achieved by adding functional fillers or particulates into SMPs. The functional fillers transform stimuli (electrical, magnetic, or optical) into thermal energy for internal material heating. The SMP nanocomposites exhibit improved mechanical and multi-stimuli-responsive properties depending on the type and loading of the nanocomposites. The carbon-based nanomaterials (i.e., carbon nanotube (CNT) and graphene oxide) and metal nanoparticles (i.e., gold and silver nanoparticles) have been used for photothermal heating of SMPs [136, 137]. For example, Yang et al. [137] used FFF printing to fabricate photoresponsive SMP containing /9 wt% carbon black (CB) in PU. Owing to the outstanding photothermal conversion efficiency of CB ($92 \pm 3\%$) [138], PU/CB composites showed high photothermal conversion efficiency. It was demonstrated the 3D-printed sunflower with photoresponsive shape memory petals can be triggered to recover its original state with light illumination of 87 mW cm^{-2}. Iron oxides (i.e., Fe_2O_3 and Fe_3O_4) and CNT have been used for inductive heating of SMPs by alternating magnetic fields [139–144]. As an example, Wei et al. [145] reported the DIW printing of UV-curable PLA/Fe_3O_4 composite for thermally and remotely actuated SMP. The composite ink viscosity

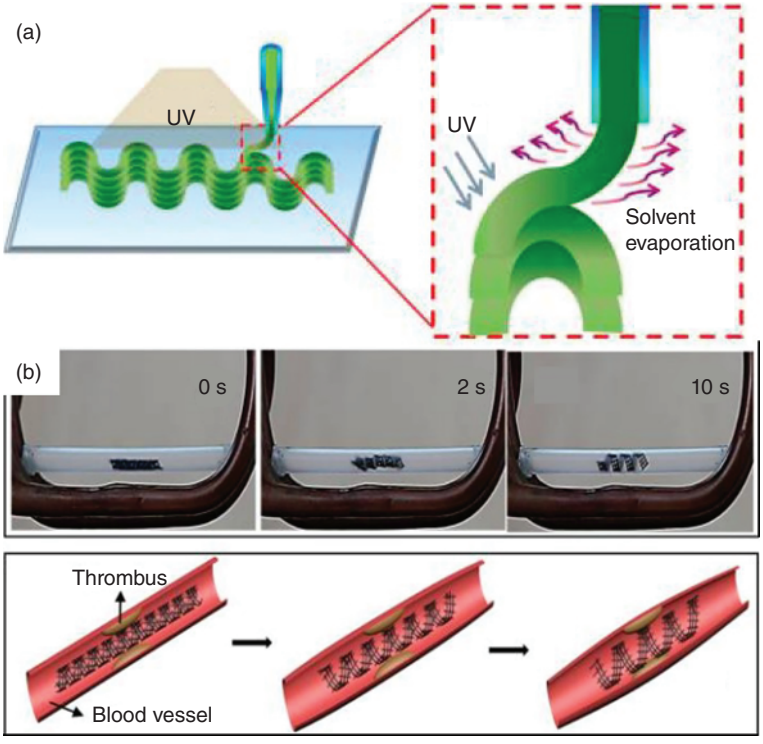

Figure 1.7 4D printing of SMP nanocomposites. (a) Schematics of extrusion of PLA/iron oxide composite ink with fast solvent evaporation and *in situ* UV crosslinking [145]. (b) Application demonstration of the 4D-printed scaffold as an intravascular stent. Source: Wei et al. [145]/with permission of American Chemical Society.

with added highly volatile solvent was extruded, followed by fast solvent removal and *in situ* UV curing (Figure 1.7a). The printed scaffolds with remote activation find potential biomedical applications as intravascular stents (Figure 1.7b). Similarly, Hua et al. [146] used FFF to print photoresponsive PLA/CNT SMP composites on paper substrates as photothermal-responsive actuators. It is also noted that, instead of utilizing nanoparticles, selectively coating colorful inks on SMPs can also realize effective photothermal heating for the activation of SMPs [117, 118].

1.3.1.3 Printed Active Fiber-Reinforced Composites

The SMP-based PACs have been extensively studied for 4D printing [2]. The bilayered PACs, fabricated by a PolyJet printer, consist of parallel glassy polymer fibers (i.e., VeroWhite) embedded in a rubbery matrix (i.e., TangoBlack). The glassy polymer fiber is an SMP with a T_g of 60 °C. After printing, the bilayer lamina was trained for shape change by heating, stretching, cooling, and releasing sequence. Finally, the composite laminates turn to curled shapes due to the strain mismatch between the rubbery matrix and the glassy polymer fibers. By regulating fiber architecture and orientation, complex 3D configurations can be obtained, including bent, coiled, twisted, and folded shapes. The SMP composites laminates were used

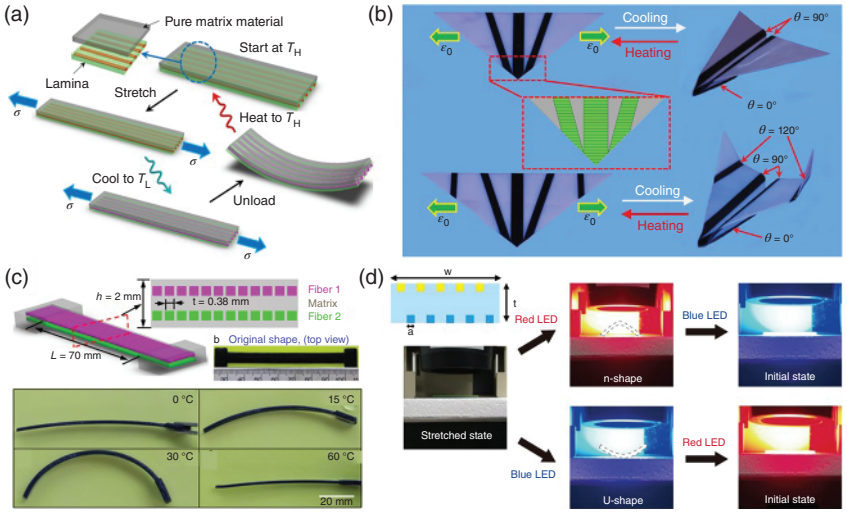

Figure 1.8 4D printing by printed active fiber-reinforced composites. (a) Schematics of the laminate architectures and shape-programming process of PAC. Source: Ge et al. [2]/with permission of AIP Publishing LLC. (b) A self-folding airplane fabricated by printing different PACs as active hinges connecting inactive stiff plates. Source: Qi et al. [17]/with permission of IOP Publishing. (c) A smart hook realized by multi-SME of PAC stripe at different temperatures. Source: Wu et al. [148]/with permission of Springer Nature. (d) Bending behavior of the multicolor PAC-based SMP composites. The composite structure has bias-distributed yellow fibers on the top and blue fibers on the bottom for selective heating under light with different wavelengths. Source: Jeong et al. [149]/with permission of Springer Nature.

as smart hinges for active origami, morphing 2D structures into 3D architectures [17, 147]. Figure 1.8b shows a 2D origami airplane with PAC-based smart hinges that can be morphed into a 3D-shaped plane [17].

Similarly, Wu et al. [148] reported the use of PACs SMP composites that shows multiple shapes change via digital SMPs. Digital SMPs with tunable T_g were printed by digital material printing on an Objet Connex printer. To do so, two materials, including a rigid plastic (VeroWhite) and a soft rubber (TangoBlack), were jetted at specific ratios, followed by UV curing to print digital materials with different T_g. With this method, SMP fibers with different T_g were printed into laminated composite structures to achieve multiple and sequential shape-shifting after a one-step shape programming (Figure 1.8c). In addition, PACs with proper arrangements can be used for metamaterial lattice, tubular grippers, and stents for self-expanding and self-shrinking shape changes [150, 151]. More recently, Jeong et al. reported 4D printing of photoresponsive PACs using selective light absorption/heating in multi-color PACs for remote-controlled shape-shifting [149]. The multi-material 3D printer (Stratasys, J750) was used to print yellow fibers (VeroYellow) and blue fibers (VeroCyan) in a rubber-like transparent material (Tango +), and the colored fibers were biasedly distributed on the top and bottom. The yellow fibers can absorb blue light, and the blue fiber absorbs red light for selective heating in the composites. As a result, the laminated composites bent to

an *n*-shape under the red light illumination and then recovered to an initial flat state by blue light illumination. The illumination blue-red light sequence enabled the structure to bend to a U-shape and recover to the initial state (Figure 1.8d).

1.3.1.4 Bilayer SMPs

Bilayer SMP composites made of SMPs as an active layer and passive rubbery layers are simple and versatile designs for shape-shifting [152]. Besides, the bilayer can be used to realize direct 4D printing, where the residual stress can be incorporated during the printing or heating step without additional shape programming. Ding et al. [153] presented the direct 4D printing of bilayer laminate by an Objet 500 Connex3 printer (Stratasys). The bilayer strip was printed by VeroClear as the SMP and TangoBlack+ (or Tango+) as the elastomer. During printing, the elastomer layer contained a compressive strain regulated by printing parameters (such as the layer printing time). The release of the residual stress led to laminate bending into new permanent shapes (Figure 1.9a). Figure 1.9b shows some typical examples of direct 4D-printed structures. The lattice with an unsymmetrical bilayer design was printed to achieve both expanding and bending upon heating. For example, upon heating, a printed flat star-shaped laminated structure and multi-layer flower could be deployed into a 3D dome shape and a blossom configuration, respectively.

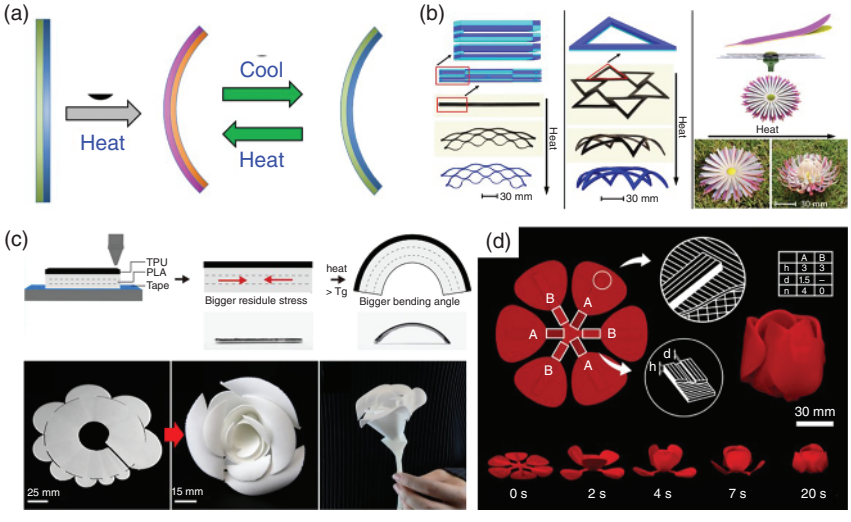

Figure 1.9 4D printing of SMP-based bilayer composites. (a) Schematics of direct 4D printing of multi-material bilayer composites. (b) Similar lattice structure with both expanding and bending upon heating with the unsymmetrical architecture. A flat star-shaped structure transforms into a 3D dome. Printed flower blooms into a blossom shape upon heating. Source: Ding et al. [153]/with permission of American Association for the Advancement of Science – AAAS. (c) FFF printing Thermorph material causes bending using an active PLA layer and passive TPU layer. A printed flat sheet self-folded into a 3D rose. Source: An et al. [154]/with permission of ACM SIGCHI. (d) FFF-printed PLA filaments with different orientations in layers can simultaneously shrink in length and thickness upon heating to a temperature above T_g. The two-step folding of the initially flat petals creates a tulip. Source: van Manen et al. [35]/from Royal Society of Chemistry/CC BY 3.0.

Ding et al. [155] further exploited the bilayer composite-based rods for direct 4D printing. Besides, the thermal expansion mismatch between the rubber and SMP layer in printed bilayer composites could also be harnessed for shape change [156]. The morphed bilayer structures were stable even after being cooled down. These examples suggested a great advantage of the 4D printing technique, which can tremendously reduce the printing time and material consumption up to 70–90% for thin-wall 3D structures.

Heat shrinkage of SMPs has also been utilized for direct 4D printing of bilayer composites without shape programming. The SMP chains (such as PLA) can be stretched and aligned along the direction of extrusion during the FFF printing process, storing internal residual stress in the polymer. Upon heating to a temperature above its T_g, the printed parts can show macroscopic contraction along the chain alignment direction due to residual stress release. For example, An et al. [154] reported the concept of Thermorph by FFF printing of bilayers consisting of an active PLA layer and a passive thermoplastic polyurethane (TPU) layer to form an actuator (Figure 1.9c). The printed 2D bilayer composites could self-fold into 3D configurations upon heating. With this Thermorph approach, complex geometries, including 3D Stanford Bunny and 3D rose, were designed, printed, and self-folded from 2D flat sheets. Zhang et al. [36] reported heat-triggered shape transformation of printed 2D lattice patterns. When the paper was used as the passive material, it could be removed after shape-shifting, yielding complex lightweight structures [157]. Besides, the heat-shrinkage property of printed SMPs can combine with geometry control for anisotropic deformation and more complex shape-shifting. Van Manen et al. [35] exploited controlled in-plane PLA filament arrangements in a one-step 3D printing process, generating various shape changes due to the heat shrinkage and the concomitant lateral expansion of the printed structure. The printing parameters (i.e., filament printing angle, component porosity, and thickness) and activation temperatures were used to tune the shrinkage of multi-ply panels (Figure 1.9d). With this method, complex shape-shifting structures, such as "sequential" shape-shifting, instability-driven pop-up, and self-folding origami, were realized.

1.3.1.5 Multi-material SMPs

3D printing of multi-material SMP is utilized for multiple and sequential shape-shifting more complex target shapes and shape evolution pathways. This was first achieved by using digital SMPs via PolyJet printing. Mao et al. [158] printed spatially distributed digital SMPs with different T_g to control the shape-shifting sequences in 3D-printed structures. Hinges composed of SMPs with higher T_g recovered slower at the same recovery temperature, leading to sequential folding. This was illustrated by self-closing and locking a box from a flat shape (Figure 1.10a). Liu et al. [160] also exploited the digital SMPs to realize programmable deployment of tensegrity structures. The shape-shifting structures find application potential as a deployable antenna, reflectors on satellites, and biomedical devices as a self-deployable stent.

Multi-material SMPs with location-specific properties can be printed by DLP with multiple switchable resin vats. Ge et al. [68] formulated different inks with tunable

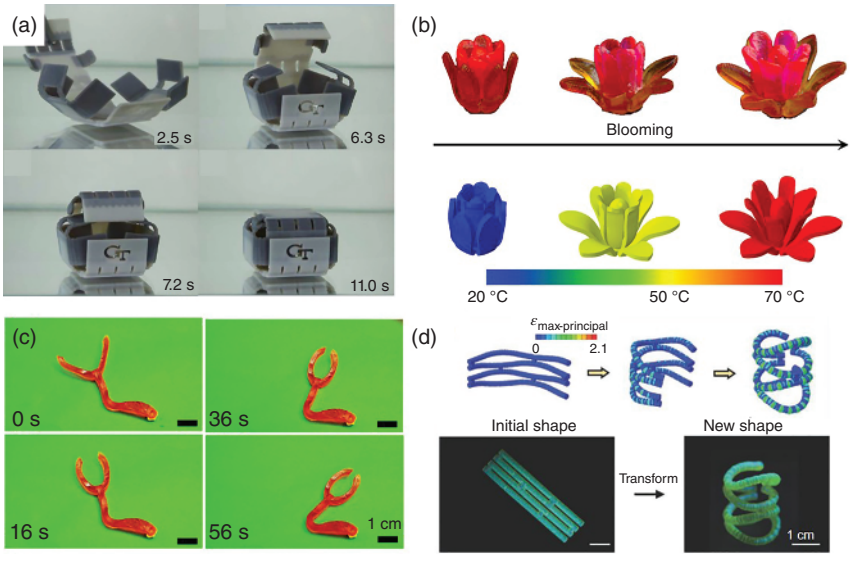

Figure 1.10 4D printing by multi-material SMPs. (a) Pictures showing the folding of a 3D-printed sheet to a box with self-locking. Source: Mao et al. [158]/with permission of Springer Nature. (b) The experiment and simulation of shape recovery of a PμSL-printed multi-material flower with different T_g for the two layers of petals. Source: Ge et al. [68]/with permission of Springer Nature. (c) Multi-material SMP for artificial arms with sequential shape recovery by grayscale DLP printing. Scale bars: 1 cm. Source: Kuang et al. [89]/with permission of American Association for the Advancement of Science – AAAS. (d) Grayscale DLP-printed shape memory balloon-based planar raft consisting of three types of hoop sequences transformed into a 3D cylindrical tent-like structure actuated by pneumatic blowing. Scale bars: 10 mm. Source: Zhang et al. [159]/with permission of John Wiley & Sons, Inc.

T_g for multi-vat PμSL printing of SMP multi-materials. As shown in Figure 1.10b, a flower was printed with two layers of petals featuring different T_g. In the programmed temporary shape of the bud state, the outer petals with lower T_g opened first after heating to 50 °C, and the inner petals with higher T_g opened at 70 °C, which can be captured by corresponding finite element (FE) simulations.

Alternatively, multi-material SMPs can be printed by grayscale DLP using a single vat [89, 159]. Compared with regular one-step grayscale DLP printing with limited mechanical properties gradients, Kuang et al. [89] reported the grayscale DLP printing of digital materials with widely tunable mechanical properties and T_g using a customized photothermal two-stage curing ink. The hybrid resin comprises a diacrylate crosslinker, a dual-functional monomer of glycidyl methacrylate (GMA), and a diamine as a thermal crosslinker. The grayscale light patterns were used during the printing stage to print green parts with locally distinct degrees of reaction conversion associated with different crosslinking densities. After printing, the green parts were further subjected to thermal curing between different functional groups. This thermal curing substantially boosted the mechanical strength and enlarged the mechanical properties contrast (Young's modulus from 1.4 MPa −1.2 GPa). In addition, the T_g can be tuned from 14 to 68 °C, which resembles the digital SMPs

obtained using a PolyJet printer. The mechanism of these widely tunable properties enabled by g-DLP lies in the variations in network architectures (such as crosslinking density and chain branches). By simply assigning grayscale levels by design, both discrete and continuous mechanical properties gradients can be printed in a single object. As a demonstration, a self-folding robot arm was printed by assigning SMPs with different T_g at the claw and elbow region to enable sequentially grabbing and then lifting a long stick in response to heat (Figure 1.10c).

Most of the previous 3D printing multi-material SMPs show relatively poor mechanical properties, and complex and precise temporary shape programming is very challenging. To resolve this issue, Zhang et al. [159] developed a novel SMP with excellent mechanical properties along with facile blow loading for multi-material 4D printing, which was termed pneumatic multi-material 4D printing. The novel ink contained isobornyl acrylate as the rigid monomer, high-molecular-weight AUD (Ebecryl 8413) as a crosslinker, and Irgacure 819 as a photoinitiator. Two SMPs with different T_g were modulated by light brightness during grayscale DLP printing. After printing, the SMP-based hollow components (or shape-memory balloons) were blown into predefined configurations under a well-controlled thermo-pneumatic condition. The shape actuation was performed at the temperature between the T_g of two SMPs so that the SMP with lower T_g was in a soft and rubbery state (Young's modulus: 0.37 MPa), while the SMP with higher T_g was still in the viscoelastic state (Young's modulus: 22.5 MPa). The significant modulus difference between these two SMPs was leveraged to realize selectively blowing of the printed parts into various shapes, which could be fixed after being cooled below the T_g of both SMPs. They showed the shape memory balloon-based planar raft transformed into a 3D cylindrical tent-like structure actuated by pneumatic blowing (Figure 1.10d).

1.3.2 Hydrogels and Composites for 4D Printing

Hydrogels are made of three-dimensional hydrophilic polymer networks that can absorb a large amount of water or fluid [161]. The hydrophilicity of hydrogels is attributed to the existence of hydrophilic functional groups (i.e., $–NH_2$, –COOH, –OH, $–CONH_2$, –CONH–, and $–SO_3H$). The water uptake and release contribute to the expansion or shrinkage of hydrogels, leading to the shape actuation. Hydrogels enable significant volume-phase transition triggered by physical and chemical stimuli (i.e., temperature, electricity, solvent composition, light, pH, and ions) [162]. Basically, the swelling equilibrium of hydrogel is determined by the crosslinking density, temperature, and interaction between the polymer chain and aqueous solution (Flory–Huggins solubility parameter). The mechanism of the stimuli-responsive reversible swelling/shrinkage of hydrogels lies in the change of polymer–water interactions. The external factors that alter the intermolecular interactions can influence the swelling state of hydrogels. Usually, single-material hydrogel shows simple expansion and contraction. To realize more complex and high-order deformation, alternating the stimulus field or using heterogeneous material structures is adopted to realize bending, twisting, and snap-buckling [163–167]. For this reason, the printing of hydrogel composites and multi-materials

is mainly used for 4D printing. This section will summarize the advances of hydrogel composites and multi-material hydrogel structures for 4D printing. More progress in the 4D printing of hydrogels can be found in the review paper [162].

1.3.2.1 Single-Material Hydrogels and Composites

Stimuli-responsive smart hydrogels and composites have been printed using different 3D printing techniques for 4D printing. Among them, the poly(*N*-isopropyl acrylamide) (PNIPAm) and its copolymers have been widely studied as temperature-sensitive hydrogels, exhibiting large and reversible volume transition at the lowest critical solution temperature (LCST, $T_C \approx 32–35\,^{\circ}C$) [168]. When increasing the temperature above T_c, the polymer network strands experience a coil–globule transition resulting in a large volume change due to the decreases in the water content [169]. Bakarich et al. [170] presented the DIW printing of ionic covalent entanglement hydrogels alginate/PNIPAm with enhanced mechanical properties and thermal actuation. A printed smart valve can realize the control of the water flow at 20 and 60 °C because the thermal-responsive hydrogel enabled the change in the size of the channel with temperature.

Polyacrylic acid (PAA) is another widely used hydrogel for 4D printing [171–173]. The presence of the carboxyl acid group enables multiple stimuli-reposing capability, including chemical, electric field, and pH [172]. Lee and coworkers [171] used PμSL to print PAA–PEG hydrogels that exhibited large deformation under electric field in an electrolyte medium (phosphate-buffered saline [PBS]). This shape-shifting was attributed to the difference in mobile ion concentrations between the inside and outside of the ionic gels. A printed human-like structure showed untethered and bidirectional locomotion under an electric field (Figure 1.11). Jin et al. [172] used TPP to print PAA-based structures with a sub-micrometer resolution for pH-triggered complex shape change.

Usually, a single hydrogel gives a limited shape deformation mode. Inspired by the complex shape change of some natural plants due to microstructural anisotropy of cell walls, composite hydrogels showing anisotropic swelling are also developed for 4D printing with complex shape-shifting behavior [174, 175]. To achieve anisotropic

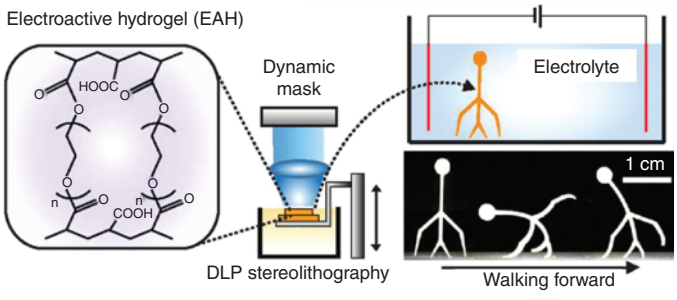

Figure 1.11 A typical example of 4D printing of single hydrogel and composite. PμSL printing PAAc-based electric active hydrogels for bidirectional locomotion human-like electroactive hydrogels (EAH) structure. Source: [171]/with permission of American Chemical Society.

swelling in hydrogel composites, micro-particulates/fillers are usually added and aligned by shearing forces [174] or external fields, such as an electric field or magnetic field [175]. For example, Gladman et al. [174] utilized DIW to print hydrogel composite using nanofibrillated cellulose (NFC) composite inks. NFC was aligned during the ink deposition process. By controlling printing pathways, the orientation of fibers in each layer could be encoded in the bilayer hydrogel structures. As a result, localized, anisotropic swelling behavior could be modulated to precisely tune the curvature of bilayer hydrogel composite structure for complex shape-shifting.

1.3.2.2 Multi-Material Hydrogels

Multi-material hydrogels with a swelling mismatch of different materials are the earliest and most extensively studied systems for complex shape change. The first 4D printing example by Tibbits is the printing of hinges composed of a rigid plastic base and a hydrogel layer using an Objet 260 Connex printer [4, 5]. The hydrogels expand upon immersion in water triggering local bending deformation. The folding angle of the hinges was precisely controlled by varying the distribution of the two materials, enabling controlled shape change. It was shown the 3D-printed multi-material strand gradually transformed into a three-dimensional cube in water with time. Using the same type of 3D printer, Mao et al. [176] further combined the SME of the SMP layer with the expansion of a hydrogel layer for 3D-printed reversible shape-changing components with enhanced mechanical properties. The multi-material printing enabled the fabrication of bilayer structures containing an SMP layer, elastomer columns, and hydrogel sandwiched between the two layers (Figure 1.12a). To allow water to flow in and out rapidly, tiny holes were positioned in the elastomer layer. When putting the structures in cold water, the deformation was constrained by the stiff SMP despite the hydrogels' swelling. Upon heating, the

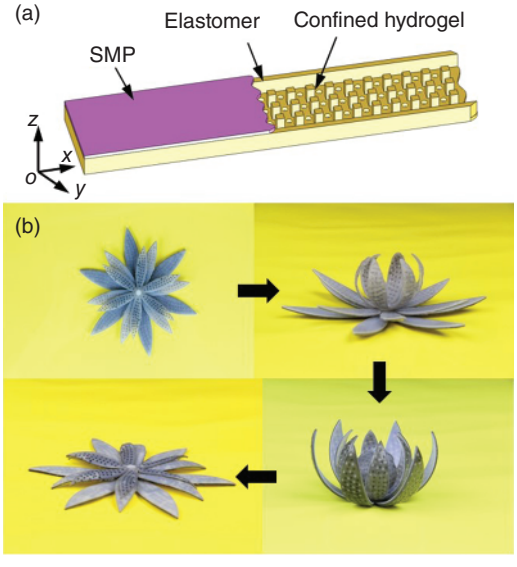

Figure 1.12 4D printing of multi-material hydrogels. (a) Schematics of 3D-printed hydrogel composite consisting of an SMP layer and a rubbery layer by PolyJet printing. (b) A printed hydrogel composites-based petal-like structure showing sequential actuation. Source: Mao et al. [176]/with permission of Springer Nature.

release of internal stress led to the structure bending due to the decreasing stiffness of SMP. The cooling and drying of the structure locked the bent shape, which recovered to the original shape after reheating. By adjusting the dimensions of the component and ratios of the two materials, the actuation speed can be tuned. Consequently, actuation of the printed flower with programmed sequences was achieved (Figure 1.12b).

DIW printing of multi-material hydrogels for 4D printing is also widely investigated. Naficy et al. [177] exploited dual-nozzle DIW printing of bilayer structures containing a thermoresponsive hydrogel (PNIPAm) and non-thermoresponsive hydrogels to realize bidirectional bending upon temperature change. Similarly, Liu et al. [178] used PNIPAm as an active layer and polyacrylamide (PAAm) as a passive layer for dual-nozzle DIW printing of biomimetic tube structures. Complex shape actuation, including radial expansion, bending, uniaxial elongation, and gripping, was realized using heat as a trigger.

DLP was used for rapid printing of multi-material hydrogels for 4D printing. Zhao et al. [166] patterned photomasks to fabricate bilayer structures with distinct physical properties and complex geometries. Hydrophilic poly(ethylene glycol) (PEGDA) was cured to form highly crosslinked hydrogels. A hydrophobic poly(propylene glycol) dimethacrylate (PPGDMA) layer was cured as a passive elastomeric layer. The resultant bilayer 2D hydrogel structures showed high actuation speed and large actuation force. In another work, Xie and coworkers [179] controlled the reaction conversion of multi-material hydrogels by adjusting the local exposure time. Shorter exposure times (or light dose) generated lower reaction conversions, leading to larger swelling ratios. With this approach, the ratio between the highest and lowest swelling ratios was as high as 40, allowing the fabrication of shapes to change with a sharp transition. Consequently, complex shape change with complex swelling patterns, such as a 3D cartoon face, was realized.

1.3.3 Liquid Crystal Elastomers

As soft-active materials, LCEs can reversibly actuate under external stimuli, such as heat or light [180–186]. LCEs comprise crosslinked polymer networks with covalently linked liquid crystals (or mesogens) in chain backbones or as side chains. Particularly, the actuation of main-chain thermal-responsive LCEs is achieved by the phase transition (nematic to isotropic) across the transition temperature (T_{NI}), which has been extensively investigated for 4D printing. By contrast, photoresponsive azobenzene-based LCEs are realized by photochemistry of *trans–cis* configuration transition under UV light illumination. The azobenzene-based LCE is less reported for 3D printing, partially attributed to the high cost of raw materials. In addition, thermal-responsive LCEs can be engineered with photo-actuation by leveraging the photothermal effect of nanoparticles [187, 188]. To facilitate large reversible shape changes, LCE mesogens are required to be aligned into a mono-domain state before use. Several alignment methods, including mechanical stretching [189–193], polarized light [186], shearing by extrusion [48–52], and magnetic fields [194], have been exploited to align the LCE mesogens. As DIW

printing enables effective mesogen alignment by the material extrusion-induced shear, DIW printing is the most widely used printing technique for 4D printing of LCEs.

1.3.3.1 Single-Material LCEs

Based on the tremendous progress in the fabrication of LCEs using aza-Michael addition chemistry [186, 195, 196], LCE ink containing viscous oligomers was printed by Ware and coworkers for the first time [48]. They synthesized a main-chain LC macromer by the Michael addition of a liquid crystal monomer, 1,4-bis-[4-(6-acryloyloxhexyloxy)benzoyloxy]-2-methylbenzene (RM82), and a chain extender, *n*-butylamine (1.1 : 1 M ratio) at 75 °C for 12 hours. The obtained LCE ink with high viscosity (~8 Pa·s at 50 s^{-1} and 85 °C) and a T_{NI} of 105 °C was DIW-printed at 85 °C. At a temperature below T_{NI}, the mesogens in the nematic regime were aligned by the shearing force during extrusion. The subsequent UV curing allowed to lock the mesogen alignment. Upon heating/cooling, the printed LCE filament exhibited reversible contraction as high as 40% strain along the printing direction. By controlling the printing path, the mesogen alignment was locally programmed. Complex shape transformations, including volumetric contractions and repetitive snap-through transitions, were realized. Soon after, Kotikian et al. [50] exploited the same strategy for 4D printing of LCE actuators with spatially programmed nematic order in arbitrary form factors for more intricate shape manipulation. A main-chain LCE ink with a lower T_{NI} of 95 °C but higher viscosity was obtained by altering the ratio of RM82 and *n*-butylamine to 1 : 1. Therefore, much higher pressure was required to operate the LCE ink printing at 50 °C. Actuation contraction of 43.6% in the printing direction and expansion of 29.8% normal to printing direction were obtained. The printed LCE-based architectures showed reversible 2D-to-3D and 3D-to-3D shape transformations. However, the actuation temperature of the above LCEs was as high as 200 °C for full actuation, limiting their actual applications.

To this end, new LCE oligomer inks have also been prepared to reduce the printing temperature or tune the actuation temperature. Researchers used soft thiol-spacers to tune the actuation temperature and realized room temperature printing of LCE by modifying the synthesis chemistry [49, 197]. In a typical example, Roach et al. [49] reported an LCE oligomer with much lower T_{NI} (42 °C) for room temperature DIW printing. The new LC ink was synthesized between a diacrylate mesogen of RM 257 and a flexible dithiol spacer 2,2′-(ethylenedioxy) diethanethiol (1.15 : 1 M ratio) in acetone with a proper catalyst. Before use, the excess acetone in the LC oligomers was evaporated under a vacuum. The extruded LC ink with aligned mesogens was cured by UV light, yielding reversible contraction actuation strain of 48% between −20 and 75 °C. Likewise, Saed et al. [51] combined the aza-Michael addition and thiol–ene reaction scheme for LCE oligomers synthesis and crosslinking. By altering the difunctional thiol's chain length and stiffness as a chain spacer, tunable actuation temperature (T_{NI}) was achieved from 28 to 105 °C. The obtained LC inks could be 3D-printed into multi-material-based structures, exhibiting sequentially and reversibly shape changes.

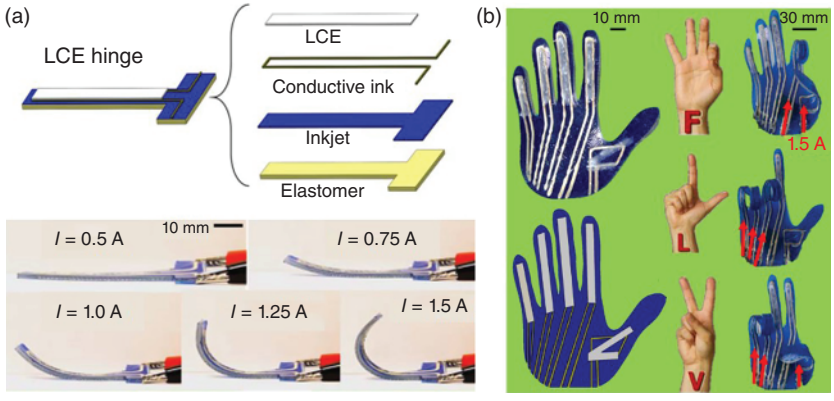

Figure 1.13 Liquid crystal elastomer (LCE)-based multi-material 4D printing. (a) Hybrid-printed multiple-layered LCE hinges connected to a power supply can be actuated to bend by Joule heating under various applied currents. (b) A fully 3D-printed LCE-based hand with individually controlled fingers to show the American sign language letters. Source: (a) and (b) Roach et al. [49]/with permission of IOP Publishing.

1.3.3.2 LCE-Based Multi-Materials

LCE-based multi-material structures containing active LCE and passive inert materials enable more complex shape change behavior. For example, Kotikian et al. [52] used DIW to print multi-LCE bilayers with orthogonal director alignment and locally different T_{NI}s to form active hinges in soft robotic structures. A self-twisting origami polyhedron and a soft robot with programmed folding sequences were realized. Roach et al. [49] also presented the printing of LCE-based multi-material electronics and metamaterials. As shown in Figure 1.13a, a rubbery substrate (1 mm) was first printed by DIW printing, and the coating layer (30 μm) was printed by inkjet printing to create a smooth surface. Then, conductive wire traces (1 mm wide, 20 μm thick) were printed and cured, followed by covering an LCE layer (0.5 mm thick) by DIW printing. When the current was applied, the conductive wire enabled Joule heating, leading to LCE contraction and bilayer bending due to the deformation constrain by the elastomer substrate. With this approach, a printed hand with individually controlled fingers could be realized, which could produce American sign language letters (Figure 1.13b). 4D-printed LCE-based structures and devices with reversible large-strain actuation, find applications as novel actuators and soft robotics [52, 198].

1.3.4 Magnetoactive Soft Materials

MSMs consisting of magnetic particles and a soft polymer matrix allow for rapid and large actuation in response to magnetic fields. The magnetically actuated shape-morphing derives from the interactions between the magnetic particles and the applied magnetic field. Two types of magnetic particles, i.e., soft and hard magnetic particles, are divided in terms of coercivity (H_c) and residual magnetic

flux density (B_r). Soft magnetic particles, such as iron and iron oxide, develop prominent magnetization and demagnetization along the external magnetic fields owning to low H_c and B_r. Therefore, soft magnetic particles-based MSM generally exhibited simple deformation modes. In contrast, hard magnetic particles, i.e., neodymium-iron-boron (NdFeB), possess very high H_c and B_r. The high remanence of hard magnetic particles enables a high B_r after magnetization to saturation [199]. When the magnetization is not in line with the external field, these embedded hard magnetic particles can exert body torques on materials, resulting in complex macroscopic shape actuation [47, 199, 200]. Therefore, the hard magnetic MSMs enable remote, fast, reversible, and untethered shape-morphing. In addition, when a time-varying magnetic field was used, complicated actuation and multi-modes of locomotion can be achieved [200, 201]. The MSMs and devices with remote-controlled actuation can find application potentials in soft robotics, biomedical devices, and active metamaterials [47, 200, 202–207]. Recent progress in the properties and applications of MSMs can be found in these review papers [99, 100]. This section discusses the progress of 3D printing of MSMs using single-material and multi-materials design.

1.3.4.1 Single Magnetoactive Soft Material Composite

Early works in the printing of MSMs mainly involve using soft magnetic materials [208]. Several recent works reported the large and complex magnetic structures using DIW printing [45, 202]. For example, Roh et al. [202] presented 3D-printed architectures with programmed magneto-capillary reconfiguration. The magnetically driven soft actuators consisting of soft silicone and carbonyl iron particles could deform easily under magnetic fields and by lateral capillary forces. Hard magnetic soft materials were also printed to enable a more complex shape-shifting mode. Kim et al. developed the magnetic field-assisted DIW printing to pattern the local magnetization by applying a magnetic field on the printing nozzle [47]. The viscous ink consisting of commercial silicone rubber (polydimethylsiloxane [PDMS]), magnetized NdFeB particles, and fumed silica as a rheological modifier was used for extrusion printing. After printing and curing, complex 2D and 3D structures with programmed magnetization enabled fast and reversible shape actuation. For example, flat sheets can repeatedly actuate into origami and recover rapidly by applying and removal of a magnetic field.

Besides, photocuring-based fabrication has been used to manufacture MSMs in small sizes [209–211]. Xu et al. [209] used UV lithography and magnetic field to manipulate the orientation of NdFeB in planar materials. Millimeter-scale flexible robots with sophisticated magnetization patterns and intricate shapes can be fabricated. It was shown that the printed multi-legged paddle-crawling robots exhibited different bending angles under magnetic actuation. The alternating magnetization profile in each leg enabled the robot's locomotion in a microchannel. In another work, Peters et al. [210] printed degradable magnetic hydrogel composites as swimming microrobots by TPP printing. The obtained microdevices absorbed and released biologically relevant substances and degraded in aqueous solutions. The magnetically actuated microdevices can be used as *in vivo*

noninvasive manual/surgical devices. Likewise, Lee et al. [211] utilized TPP to print size-controllable superparamagnetic hydrogel for the fabrication of microscrews and microrollers that could respond to diverse stimuli, including magnetic field, pH, temperature, and cations.

1.3.4.2 Multi-material MSMs

Multi-material 4D printing has been achieved to further enhance the functionality of MSMs. Li et al. [212] used switchable resin vat DLP printing for DLP printing of multi-materials and devices. A magnetic field actuated flexible gripper with integrated magnetic-responsive, and inert materials can be printed into a single part. The magnetic composite photopolymer ink contained Fe_3O_4 nanoparticles. A simple match-like actuator contains the top head printed by magnetic resin and a thin load-bearing piece. The dual-material DLP printing enables good surface quality and interfacial bonding for effective actuation. A printed flexible gripper could pick up and release a cotton ball in response to magnetic fields.

Recently, Ma et al. [43] used multi-material DIW printing to fabricate complex structures consisting of photocurable magnetic shape memory polymers (M-SMPs) and MSMs (Figure 1.14). The M-SMP is made of an AUD-based photopolymer and NdFeB microparticles, which combines the advantages of MSMs and SMPs [144]. Fumed silica nanoparticles as a rheological modifier were also added to impart

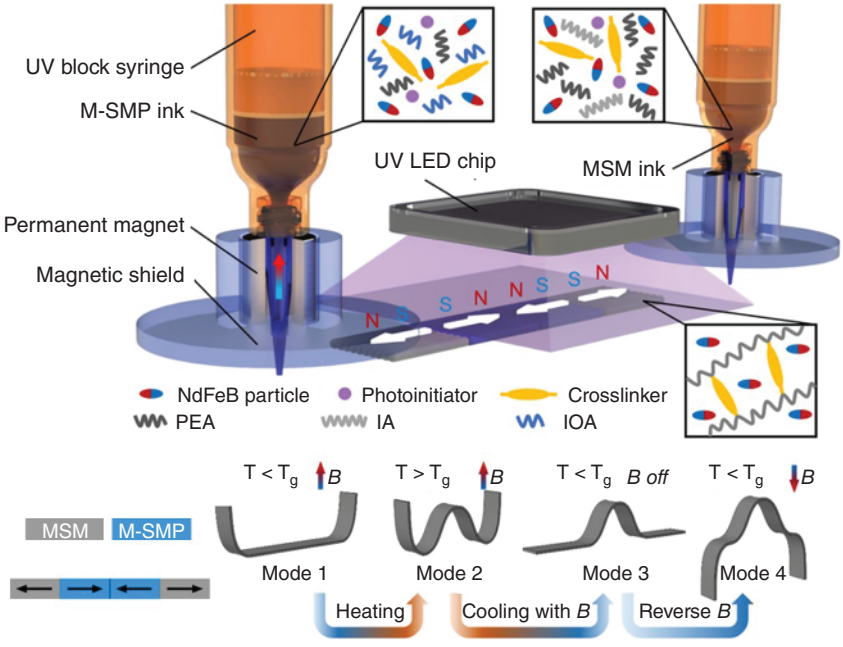

Figure 1.14 4D printing by MSMs-based multi-material. Schematic of the magnetic multi-material DIW system to print two magnetoactive materials with different glass transition temperatures. Cooperatively controlling the temperature and magnetic field led to different deformation modes. Source: Ma et al. [43]/with permission of American Chemical Society.

shearing shining for extrusion. To make MSM with low glass transition temperature, a rigid monomer (isobornyl acrylate) was replaced by a flexible monomer (isodecyl acrylate). 2D lattice structures exhibited multimodal shape actuation and tunable physical properties through cooperative heating and magnetic field control. For example, only the MSM parts (T_g below room temperature) could be actuated at room temperature by the magnetic field, and the stiff M-SMP parts could be kept undeformed state. Upon heating above T_g, both materials were activated for the magnetic actuation. In addition, the M-SMP parts could lock the deformed shape after cooling down, which was stable without magnetic field. The locked shape could still recover upon heating due to the SME of the M-SMP.

1.4 Modeling-Guided Design for 4D Printing

Mechanics modeling and multiphysics simulation-based approaches play a vital role in predicting the shape-shifting and guiding the design in 4D printing. For bilayer structure-based 4D printing involving simple expansion and shrinkage, the beam theory and its modified models have been extensively employed to predict the shape-shifting [102, 103, 166, 213]. For example, Boley et al. reported the precise and complex shape manipulation of multiplex bilayer lattices via the mechanics model-guided multi-material 4D printing [103]. In addition, the beam theory has been extended to voxelized 3D object's deformation, such as a lattice frame, to capture the object's deformed shape in bulk materials [214].

To predict the complex shape-shifting in smart materials, multiphysics-based simulations are usually required to capture all relevant physical processes before, during, and after the shape-shifting. Different physical processes, including thermal, electromagnetic, chemical reactions, photochemistry, or a combination of these physical processes, may be involved. Different constitutive models of smart programmable material systems, including SMPs [148, 153, 215–219], LCEs [220–222], hydrogel composites [165, 223–225], and magnetic materials [47, 199], have been established. Using the well-developed materials models, a designer can design the material with the model-based finite element method to study the influence of material distributions and programming strategies. For example, Zhao et al. [199] used simulations to guide the design of MSMs with programmed magnetization patterns for target shape actuation (Figure 1.15a). However, this intuition-based design can be tedious, and large sets of possibilities exist for a particular design due to many tunable parameters.

The recent progress in computer-based methods to design shape-programmable structures for 4D printing has been achieved via machine learning (ML). Genetic algorithms (GAs), also known as evolutionary algorithms (EAs), are typical ML methods. EA is population-based gradient-free optimization, which is well suitable for searching problems-based optimization. For the design problem in 4D printing, EA can be used to search the complex design of active material distribution. Based on a predefined criterion, the ideal material distribution can be found by selecting the best-performing designs to continue reproducing and discarding the most inferior performing designs in an iteration manner. For example, Sossou et al. [228]

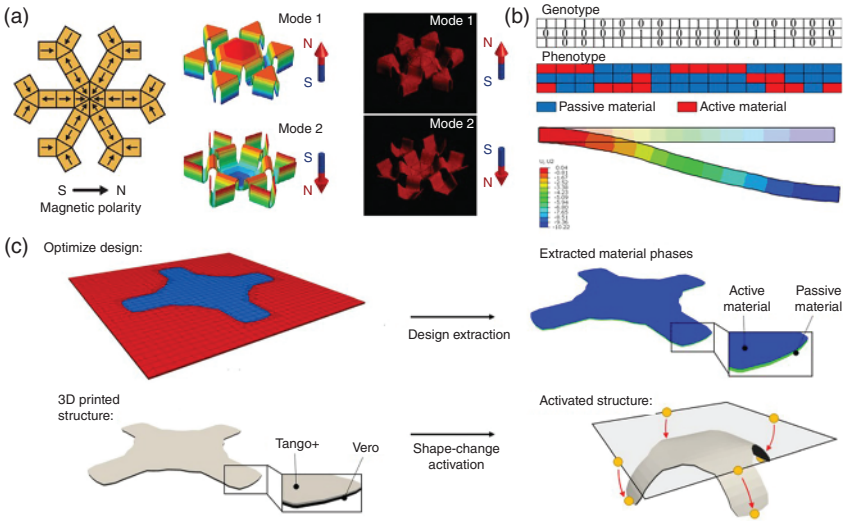

Figure 1.15 Simulation-based design for 4D printing. (a) An FE-based model-guided design of shape-shifting structures with programmed patterns of ferromagnetic domains for 3D-printed MSMs [199]. (b) Schematic illustration of genetic algorithm representing active materials (red) and passive materials (blue) in the phenotype to realize a target deformation [226]. (c) A level-set topology optimization approach for 4D printing using digital materials. Source: Geiss et al. [227]/with permission of American Society of Mechanical Engineers (ASME).

reported an EA-based modeling framework to simulate the materials in a voxelized manner. The initial shape was first voxelized and meshed with a chosen resolution. Secondly, the voxelized source shape and target deformation mode were compared to get the necessary underlying frame nodes' rotational degrees of freedom for the target shape. Lastly, the inverse design problem was solved by MATLAB toolbox, yielding the optimal material distribution design. The simulations with reasonable simulation speed can be used to predict the shape change of complex 3D structures. In another work, Hamel et al. [226] utilized the EA to guide the active material composite design in 4D printing. EA was combined with the finite element method to solve multi-material design optimization problems for target shape-shifting. To do so, the discrete passive or active materials were voxelized. As indicated by the "phenotype," their distribution was optimized to reach predetermined configuration by multiple-generation iterations (Figure 1.15b). When the active composite configuration matched the target shape as the best results, the corresponding material distribution indicated the optimized active material design. More recently, Wu et al. [46] reported EA-assisted voxel-encoding for DIW printing to control both the magnetic density and polarity direction distributions in MSMs. The simulation-guided design for 4D printing of MSMs enabled complicated and on-demand shape-morphing.

Besides, topology optimization (TO) provides another robust tool for material distribution optimization in 4D printing design. In a TO process, a continuous function is used to represent the distribution of discrete material [229, 230].

Recently, TO has been used to optimize the material distribution in multi-material 4D printing. For example, Dunn and coworkers [231] reported the use of the level set approach and the extended finite element method in combination with density-based TO to solve the multi-material optimization problem (Figure 1.15c). In addition, the extension of TO to large-deformation design optimization could broaden materials applied [227]. However, TO is not suitable to capture complex multiphysics with nonlinear material properties and geometry.

1.5 Summary and Outlook

4D printing allows the 3D-printed structures and devices to change their shapes and properties under external triggers after printing. The advances of various shape-programmable materials, multi-material printing techniques, and design tools have driven the emergence and rapid development of 4D printing since 2013. SMP composites and nanocomposites are the widely used material systems for 4D printing. Multi-material SMPs further expand the shape-shifting mode and complexity. However, 4D-printed SMPs usually showed irreversible shape-shifting. By contrast, hydrogel composites with stimuli-responsive swelling and contraction enable reversible shape-shifting by the water uptake/release. The major limitations of hydrogels are their slow actuation due to the diffusion-induced volume change and the weak mechanical properties. LCEs exhibit reversible actuation and enhanced mechanical properties compared with hydrogels. MSMs are emerging smart materials with remote-controlled, untethered, and fast actuation. 4D printing of SMPs, hydrogel, and MSMs is compatible with various single-material and multi-material printing modalities. However, 4D printing of LCEs requires the mesogens to be aligned, which is currently limited to extrusion-based printing. 4D printing using smart materials exhibits several unique features complementing advanced manufacturing and also enables functional properties. Therefore, 4D printing has become one of the fasting-growing techniques, attracting broad attention to multidiscipline.

For future materials in 4D printing, printable smart materials with robust physical properties for extreme conditions, multi-stimuli-responsive, sensing-actuation-integrated intelligence, and excellent bioactivity can be developed to satisfy different applications. In aerospace, 4D-printed programmable materials usually possess large sizes, outstanding mechanical/thermomechanical properties, long-service lifespans, and tolerance to extreme space conditions. To this end, mechanically robust SMPs exhibiting high service temperature and excellent environmental stability are desired. One interesting trend in material design is the integrated multifunctions of smart programmable materials. For instance, the common elastomeric matrix of MSMs can be replaced by SMPs, hydrogels, or LCEs, which can expand the functional properties of MSMs [144, 232]. Another emerging functional programmable material is vitrimer (or covalent adaptive networks), which is capable of rearranging the network via dynamic chemical reactions [232–236]. The stimuli-induced plasticity enables sustainable applications via repeatable programmability, recycling, and self-healing for 4D printing [237–241].

More robust design methods, particularly the simulation-based design tools, can empower the design for 4D printing. The biomimetic concept can provide great inspiration for the design in 4D printing [242–244]. In terms of simulation-guided design, ML offers a powerful tool to design structures with multiphysics involving geometric and material nonlinearity that is usually challenging through traditional approaches. The simulation/modeling approaches also provide a nonintuitive solution to inverse design problems [201, 214]. In addition, TO has been used to optimize the design of smart structures with reduced weight.

Lastly, the rapid development of new 3D printing techniques will no doubt advance the 4D printing technique. Multiscale-geometry, high-speed, and multi-material printing will play a critical role in future 4D printing techniques. Recent progress of volumetric 3D printing can tremendously improve the printing speed [245–248], while high-area rapid printing can increase the printing size enormously [249]. In addition, external fields (such as electric fields and magnetic fields) have been combined with 3D printing, allowing the fabrication of anisotropic stimuli-responsive smart materials for 4D printing [250, 251]. With this interdisciplinary research progress, 4D printing can transform into a practical technique, finding applications in broad fields such as soft robots, aerospace, biomedical devices, and more.

Acknowledgments

H.J.Q. acknowledges the support of AFOSR grants (FA9550-19-1-0151 and FA9550-20-1-0306; Dr. B.-L. "Les" Lee, Program Manager) and a gift fund from HP, Inc.

References

1 Tibbits, S. (2013). The emergence of "4D printing". https://www.ted.com/talks/skylar_tibbits_the_emergence_of_4d_printing (accessed 26 June 2022).
2 Ge, Q., Qi, H.J., and Dunn, M.L. (2013). Active materials by four-dimension printing. *Applied Physics Letters* 103 (13): 131901.
3 Momeni, F., Mehdi Hassani, S.M., Liu, X. et al. (2017). A review of 4D printing. *Materials & Design* 122: 42–79.
4 Tibbits, S. (2014). 4D printing: multi-material shape change. *Architectural Design* 84 (1): 116–121.
5 Raviv, D., Zhao, W., McKnelly, C. et al. (2014). Active printed materials for complex self-evolving deformations. *Scientific Reports* 4: 7422.
6 Pei, E. (2014). 4D printing: dawn of an emerging technology cycle. *Assembly Automation* 34 (4): 310–314.
7 Kuang, X., Roach, D.J., Wu, J. et al. (2018). Advances in 4D printing: materials and applications. *Advanced Functional Materials* 29 (2): 1805290.
8 Choi, J., Kwon, O.C., Jo, W. et al. (2015). 4D printing technology: a review. *3D Printing and Additive Manufacturing* 2 (4): 159–167.

9 Wu, J.-J., Huang, L.-M., Zhao, Q. et al. (2017). 4D printing: history and recent progress. *Chinese Journal of Polymer Science* 36 (5): 563–575.

10 Shin, D.-G., Kim, T.-H., and Kim, D.-E. (2017). Review of 4D printing materials and their properties. *International Journal of Precision Engineering and Manufacturing-Green Technology* 4 (3): 349–357.

11 Khoo, Z.X., Teoh, J.E.M., Liu, Y. et al. (2015). 3D printing of smart materials: a review on recent progresses in 4D printing. *Virtual and Physical Prototyping* 10 (3): 103–122.

12 Stansbury, J.W. and Idacavage, M.J. (2016). 3D printing with polymers: challenges among expanding options and opportunities. *Dental Materials* 32 (1): 54–64.

13 Huang, S.H., Liu, P., Mokasdar, A. et al. (2013). Additive manufacturing and its societal impact: a literature review. *The International Journal of Advanced Manufacturing Technology* 67 (5): 1191–1203.

14 Ma, J., Franco, B., Tapia, G. et al. (2017). Spatial control of functional response in 4D-printed active metallic structures. *Scientific Reports* 7: 46707.

15 Bargardi, F.L., Le Ferrand, H., Libanori, R. et al. (2016). Bio-inspired self-shaping ceramics. *Nature Communications* 7: 13912.

16 Liu, G., Zhao, Y., Wu, G. et al. (2018). Origami and 4D printing of elastomer-derived ceramic structures. *Science Advances* 4 (8).

17 Qi, G., Conner, K.D., Qi, H.J. et al. (2014). Active origami by 4D printing. *Smart Materials and Structures* 23 (9): 094007.

18 Lui, Y.S., Sow, W.T., Tan, L.P. et al. (2019). 4D printing and stimuli-responsive materials in biomedical aspects. *Acta Biomaterialia*.

19 Li, Y.-C. et al. (2016). 4D bioprinting: the next-generation technology for biofabrication enabled by stimuli-responsive materials. *Biofabrication* 9 (1): 012001.

20 Zhang, Z., Demir, K.G., and Gu, G.X. (2019). Developments in 4D-printing: a review on current smart materials, technologies, and applications. *International Journal of Smart and Nano Materials* 10 (3): 205–224.

21 Zolfagharian, A., Kaynak, A., and Kouzani, A. (2020). Closed-loop 4D-printed soft robots. *Materials & Design* 188: 108411.

22 Pei, E. and Loh, G.H. (2018). Technological considerations for 4D printing: an overview. *Progress in Additive Manufacturing* 3 (1): 95–107.

23 Gao, B., Yang, Q., Zhao, X. et al. (2016). 4D bioprinting for biomedical applications. *Trends in Biotechnology* 34 (9): 746–756.

24 Montgomery, S.M., Kuang, X., Armstrong, C.D. et al. (2020). Recent advances in additive manufacturing of active mechanical metamaterials. *Current Opinion in Solid State and Materials Science* 24 (5): 100869.

25 González-Henríquez, C.M., Sarabia-Vallejos, M.A., and Rodriguez-Hernandez, J. (2019). Polymers for additive manufacturing and 4D-printing: materials, methodologies, and biomedical applications. *Progress in Polymer Science* 94: 57–116.

26 Ryan, K.R., Down, M.P., and Banks, C.E. (2020). Future of additive manufacturing: overview of 4D and 3D printed smart and advanced materials and their applications. *Chemical Engineering Journal* 126162.

27 Peng, B., Yang, Y., and Cavicchi, K.A. (2020). Sequential shapeshifting 4D printing: programming the pathway of multi-shape transformation by 3D printing stimuli-responsive polymers. *Multifunctional Materials* 3 (4): 042002.

28 Shen, B., Erol, O., Fang, L. et al. (2020). Programming the time into 3D printing: current advances and future directions in 4D printing. *Multifunctional Materials* 3 (1): 012001.

29 Spiegel, C.A., Hippler, M., Münchinger, A. et al. 4D printing at the microscale. *Advanced Functional Materials* 30 (26): 1907615.

30 International Organization for Standardization/ASTM International (2015). *Additive manufacturing — General principles — Terminology (ISO/ASTM 52900)*.

31 Kuang, X. (2021). Chapter 9 – Introduction to 4D printing: methodologies and materials. In: *Additive Manufacturing* (ed. J. Pou, A. Riveiro and J.P. Davim), 303–342. Elsevier.

32 Ligon, S.C., Liska, R., Stampfl, J. et al. (2017). Polymers for 3D printing and customized additive manufacturing. *Chemical Reviews* 117 (15): 10212–10290.

33 Mukherjee, T., Zhang, W., and DebRoy, T. (2017). An improved prediction of residual stresses and distortion in additive manufacturing. *Computational Materials Science* 126: 360–372.

34 Jia, D., Li, F., and Zhang, Y. (2020). 3D-printing process design of lattice compressor impeller based on residual stress and deformation. *Scientific Reports* 10 (1): 600.

35 van Manen, T., Janbaz, S., and Zadpoor, A.A. (2017). Programming 2D/3D shape-shifting with hobbyist 3D printers. *Materials Horizons* 4 (6): 1064–1069.

36 Zhang, Q., Yan, D., Zhang, K. et al. (2015). Pattern transformation of heat-shrinkable polymer by three-dimensional (3D) printing technique. *Scientific Reports* 5: 8936.

37 Tao, Y., J. Gu, B. An, et al. (2018). Demonstrating thermorph: democratizing 4D printing of self-folding materials and interfaces. In: *Extended Abstracts of the 2018 CHI Conference on Human Factors in Computing Systems*. ACM.

38 Hansen, C.J., Saksena, R., Kolesky, D.B. et al. (2013). High-throughput printing via microvascular multinozzle arrays. *Advanced Materials* 25 (1): 96–102.

39 Chen, K., Kuang, X., Li, V. et al. (2018). Fabrication of tough epoxy with shape memory effects by UV-assisted direct-ink write printing. *Soft Matter* 14 (10): 1879–1886.

40 Compton, B.G. and Lewis, J.A. (2014). 3D-printing of lightweight cellular composites. *Advanced Materials* 26 (34): 5930–5935.

41 Invernizzi, M., Natale, G., Levi, M. et al. (2016). UV-assisted 3D printing of glass and carbon fiber-reinforced dual-cure polymer composites. *Materials* 9 (7): 583.

42 Lebel, L.L., Aissa, B., Khakani, M.A.E. et al. (2010). Ultraviolet-assisted direct-write fabrication of carbon nanotube/polymer nanocomposite microcoils. In: *Advanced Materials*, 592–596. Wiley-VCH Verlag.

43 Ma, C., Wu, S., Ze, Q. et al. (2020). Magnetic multimaterial printing for multimodal shape transformation with tunable properties and shiftable mechanical Behaviors. *ACS Applied Materials & Interfaces* 13 (11): 12639–12648.

44 Zhang, Y., Wang, Q., Yi, S. et al. (2021). 4D printing of magnetoactive soft materials for on-demand magnetic actuation transformation. *ACS Applied Materials & Interfaces* 13 (3): 4174–4184.

45 Zhu, P., Yang, W., Wang, R. et al. (2018). 4D printing of complex structures with a fast response time to magnetic stimulus. *ACS Applied Materials & Interfaces* 10 (42): 36435–36442.

46 Wu, S., Hamel, C.M., Ze, Q. et al. (2020). Evolutionary algorithm-guided voxel-encoding printing of functional hard-magnetic soft active materials. *Advanced Intelligent Systems* 2 (8): 2000060.

47 Kim, Y., Yuk, H., Zhao, R. et al. (2018). Printing ferromagnetic domains for untethered fast-transforming soft materials. *Nature* 558 (7709): 274–279.

48 Ambulo, C.P., Burroughs, J.J., Boothby, J.M. et al. (2017). Four-dimensional printing of liquid crystal elastomers. *ACS Applied Materials & Interfaces* 9 (42): 37332–37339.

49 Roach, D.J., Kuang, X., Yuan, C. et al. (2018). Novel ink for ambient condition printing of liquid crystal elastomers for 4D printing. *Smart Materials and Structures* 27 (12): 125011.

50 Kotikian, A., Truby, R.L., Boley, J.W. et al. (2018). 3D printing of liquid crystal elastomeric actuators with spatially programed nematic order. *Advanced Materials* 30 (10): 1706164.

51 Saed, M.O., Ambulo, C.P., Kim, H. et al. (2019). Molecularly-engineered, 4D-printed liquid crystal elastomer actuators. *Advanced Functional Materials* 29 (3): 1806412.

52 Kotikian, A., McMahan, C., Davidson, E.C. et al. (2019). Untethered soft robotic matter with passive control of shape morphing and propulsion. *Science Robotics* 4: eaax7044.

53 Wang, Z., Wang, Z., Zheng, Y. et al. (2020). Three-dimensional printing of functionally graded liquid crystal elastomer. *Science Advances* 6 (39): eabc0034.

54 Gao, X., Qi, S., Kuang, X. et al. (2020). Fused filament fabrication of polymer materials: a review of interlayer bond. *Additive Manufacturing* 101658.

55 de Gans, B.J., Duineveld, P.C., and Schubert, U.S. (2004). Inkjet printing of polymers: state of the art and future developments. *Advanced Materials* 16 (3): 203–213.

56 Cazón, A., Morer, P., and Matey, L. (2014). PolyJet technology for product prototyping: tensile strength and surface roughness properties. *Proceedings of the Institution of Mechanical Engineers, Part B: Journal of Engineering Manufacture* 228 (12): 1664–1675.

57 Barclift, M.W. and Williams, C.B. (2012). Examining variability in the mechanical properties of parts manufactured via polyjet direct 3D printing.

In: *International Solid Freeform Fabrication Symposium*. University of Texas at Austin Austin, Texas.

58 Jang, D., Kim, D., and Moon, J. (2009). Influence of fluid physical properties on ink-jet printability. *Langmuir* 25 (5): 2629–2635.

59 Sun, C., Fang, N., Wu, D. et al. (2005). Projection micro-stereolithography using digital micro-mirror dynamic mask. *Sensors and Actuators A: Physical* 121 (1): 113–120.

60 Janusziewicz, R., Tumbleston, J.R., Quintanilla, A.L. et al. (2016). Layerless fabrication with continuous liquid interface production. *Proceedings of the National Academy of Sciences of the United States of America* 113 (42): 201605271.

61 Tumbleston, J.R., Shirvanyants, D., Ermoshkin, N. et al. (2015). Continuous liquid interface production of 3D objects. *Science* 347 (6228): 1349–1352.

62 Qi, G., Zhiqin, L., Zhaolong, W. et al. (2020). Projection micro stereolithography based 3D printing and its applications. *International Journal of Extreme Manufacturing*.

63 Mao, M., He, J., Li, X. et al. (2017). The emerging Frontiers and applications of high-resolution 3D printing. *Micromachines* 8 (4): 113.

64 Rafiee, M., Farahani, R.D., and Therriault, D. (2020). Multi-material 3D and 4D printing: a survey. *Advanced Science* 7 (12): 1902307.

65 Zhang, Y.-F., Zhang, N., Hingorani, H. et al. (2019). Fast-response, stiffness-tunable soft actuator by hybrid multimaterial 3D printing. *Advanced Functional Materials* 29 (15): 1806698.

66 Kokkinis, D., Bouville, F., and Studart, A.R. (2018). 3D printing of materials with tunable failure via bioinspired mechanical gradients. *Advanced Materials* 30 (19): 1705808-n/a.

67 Skylar-Scott, M.A., Mueller, J., Visser, C.W. et al. (2019). Voxelated soft matter via multimaterial multinozzle 3D printing. *Nature* 575 (7782): 330–335.

68 Ge, Q., Sakhaei, A.H., Lee, H. et al. (2016). Multimaterial 4D printing with tailorable shape memory polymers. *Scientific Reports* 6: 31110.

69 MacDonald, E. and Wicker, R. (2016). Multiprocess 3D printing for increasing component functionality. *Science* 353 (6307).

70 Bakarich, S.E., Gorkin, R. III, Gately, R. et al. (2017). 3D printing of tough hydrogel composites with spatially varying materials properties. *Additive Manufacturing* 14: 24–30.

71 Li, V.C.-F., Kuang, X., Hamel, C.M. et al. (2019). Cellulose nanocrystals support material for 3D printing complexly shaped structures via multi-materials-multi-methods printing. *Additive Manufacturing* 28: 14–22.

72 Espalin, D., Ramirez, J.A., Medina, F. et al. (2014). Multi-material, multi-technology FDM: exploring build process variations. *Rapid Prototyping Journal* 20 (3): 236–244.

73 Xu, C., Quinn, B., Lebel, L.L. et al. (2019). Multi-material direct ink writing (DIW) for complex 3D metallic structures with removable supports. *ACS Applied Materials & Interfaces* 11 (8): 8499–8506.

74 Hardin, J.O., Ober, T.J., Valentine, A.D. et al. (2015). Microfluidic printheads for multimaterial 3D printing of viscoelastic inks. *Advanced Materials* 27 (21): 3279–3284.

75 Ren, L., Song, Z., Liu, H. et al. (2018). 3D printing of materials with spatially non-linearly varying properties. *Materials & Design* 156: 470–479.

76 Miriyev, A., Xia, B., Joseph, J.C. et al. (2019). Additive manufacturing of silicone composites for soft actuation. *3D Printing and Additive Manufacturing* 6 (6): 309–318.

77 Ortega, J.M., Golobic, M., Sain, J.D. et al. (2019). Active mixing of disparate inks for multimaterial 3D printing. *Advanced Materials Technologies* 4 (7): 1800717.

78 Chen, K., Zhang, L., Kuang, X. et al. (2019. **0**(0)). Dynamic photomask-assisted direct ink writing multimaterial for multilevel triboelectric nanogenerator. *Advanced Functional Materials* 1903568.

79 Jochen, M., Diana, C., Manuel, S. et al. (2017). Mechanical properties of interfaces in inkjet 3D printed single- and multi-material parts. *3D Printing and Additive Manufacturing* 4 (4): 193–199.

80 Choi, J.-W., MacDonald, E., and Wicker, R. (2010). Multi-material microstereolithography. *The International Journal of Advanced Manufacturing Technology* 49 (5-8): 543–551.

81 Kowsari, K., Akbari, S., Wang, D. et al. (2018). High-efficiency high-resolution multimaterial fabrication for digital light processing-based three-dimensional printing. *3D Printing and Additive Manufacturing* 5 (3): 185–193.

82 Ge, Q., Chen, Z., Cheng, J. et al. (2021). 3D printing of highly stretchable hydrogel with diverse UV curable polymers. *Science Advances* 7 (2): eaba4261.

83 Dolinski, N.D., Page, Z.A., Callaway, E.B. et al. (2018). Solution mask liquid lithography (SMaLL) for one-step, multimaterial 3D printing. *Advanced Materials* 30 (31): 1800364.

84 Schwartz, J.J. and Boydston, A.J. (2019). Multimaterial actinic spatial control 3D and 4D printing. *Nature Communications* 10 (1): 791.

85 Peterson, G.I., Schwartz, J.J., Zhang, D. et al. (2016). Production of materials with spatially-controlled cross-link density via vat photopolymerization. *ACS Applied Materials & Interfaces* 8 (42): 29037–29043.

86 Na, J.-H., Bende, N.P., Bae, J. et al. (2016). Grayscale gel lithography for programmed buckling of non-Euclidean hydrogel plates. *Soft Matter* 12 (22): 4985–4990.

87 Zhao, Z., Wu, J., Mu, X. et al. (2017). Origami by frontal photopolymerization. *Science Advances* 3 (4): e1602326.

88 Jiangtao, W., Zeang, Z., Xiao, K. et al. (2018). Reversible shape change structures by grayscale pattern 4D printing. *Multifunctional Materials* 1 (1): 015002.

89 Kuang, X., Wu, J., Chen, K. et al. (2019). Grayscale digital light processing 3D printing for highly functionally graded materials. *Science Advances* 5 (5): eaav5790.

90 Medina, F., A. Lopes, A. Inamdar, et al. (2005). *Hybrid manufacturing: integrating direct-write and stereolithography. Proceedings of the 2005 solid freeform fabrication*, p. 39–49.

91 Peng, X., Kuang, X., Roach, D.J. et al. (2021). Integrating digital light processing with direct ink writing for hybrid 3D printing of functional structures and devices. *Additive Manufacturing* 40: 101911.

92 Roach, D.J., Hamel, C.M., Dunn, C.K. et al. (2019). The m4 3D printer: a multi-material multi-method additive manufacturing platform for future 3D printed structures. *Additive Manufacturing* 29: 100819.

93 Kuang, X., Roach, D.J., Hamel, C.M. et al. (2020). Materials, design, and fabrication of shape programmable polymers. *Multifunctional Materials* 3 (3).

94 Hu, J., Zhu, Y., Huang, H. et al. (2012). Recent advances in shape–memory polymers: structure, mechanism, functionality, modeling and applications. *Progress in Polymer Science* 37 (12): 1720–1763.

95 Xie, H., Yang, K.-K., and Wang, Y.-Z. (2019). Photo-cross-linking: a powerful and versatile strategy to develop shape-memory polymers. *Progress in Polymer Science* 95: 32–64.

96 Erol, O., Pantula, A., Liu, W. et al. (2019). Transformer hydrogels: a review. *Advanced Materials Technologies* 4 (4): 1900043.

97 Ula, S.W., Traugutt, N.A., Volpe, R.H. et al. (2018). Liquid crystal elastomers: an introduction and review of emerging technologies. *Liquid Crystals Reviews* 6 (1): 78–107.

98 White, T.J. and Broer, D.J. (2015). Programmable and adaptive mechanics with liquid crystal polymer networks and elastomers. *Nature Materials* 14 (11): 1087–1098.

99 Nguyen, V.Q., Ahmed, A.S., and Ramanujan, R.V. (2012). Morphing soft magnetic composites. *Advanced Materials* 24 (30): 4041–4054.

100 Wu, S., Hu, W., Ze, Q. et al. (2020). Multifunctional magnetic soft composites: a review. *Multifunctional Materials* 3 (4): 042003.

101 Zhang, Q., Kuang, X., Weng, S. et al. (2020). Rapid volatilization induced mechanically robust shape-morphing structures toward 4D printing. *ACS Applied Materials & Interfaces* 12 (15): 17979–17987.

102 Weng, S., Kuang, X., Zhang, Q. et al. (2021). 4D printing of glass fiber-regulated shape shifting structures with high stiffness. *ACS Applied Materials & Interfaces* 13 (11): 12797–12804.

103 Boley, J.W., van Rees, W.M., Lissandrello, C. et al. (2019). Shape-shifting structured lattices via multimaterial 4D printing. *Proceedings of the National Academy of Sciences of the United States of America* 116 (42): 20856–20862.

104 Behl, M., Razzaq, M.Y., and Lendlein, A. (2010). Multifunctional shape-memory polymers. *Advanced Materials* 22 (31): 3388–3410.

105 Mather, P.T., Luo, X., and Rousseau, I.A. (2009). Shape memory polymer research. *Annual Review of Materials Research* 39: 445–471.

106 Lendlein, A. and Gould, O.E.C. (2019). Reprogrammable recovery and actuation behaviour of shape-memory polymers. *Nature Reviews Materials* 4 (2): 116–133.

107 Hager, M.D., Bode, S., Weber, C. et al. (2015). Shape memory polymers: past, present and future developments. *Progress in Polymer Science* 49–50(0): 3–33.
108 Liu, Y., Genzer, J., and Dickey, M.D. (2016). "2D or not 2D": shape-programming polymer sheets. *Progress in Polymer Science* 52: 79–106.
109 Zhao, Q., Qi, H.J., and Xie, T. (2015). Recent progress in shape memory polymer: new behavior, enabling materials, and mechanistic understanding. *Progress in Polymer Science* 49-50(0): 79–120.
110 Liu, Y., Li, Y., Yang, G. et al. (2015). Multi-stimulus-responsive shape-memory polymer nanocomposite network cross-linked by cellulose nanocrystals. *ACS Applied Materials & Interfaces* 7 (7): 4118–4126.
111 Fang, Y., Ni, Y., Choi, B. et al. (2015). Chromogenic photonic crystals enabled by novel vapor-responsive shape-memory polymers. *Advanced Materials* 27 (24): 3696–3704.
112 Huang, W., Yang, B., An, L. et al. (2005). Water-driven programmable polyurethane shape memory polymer: demonstration and mechanism. *Applied Physics Letters* 86 (11): 114105.
113 Guo, Y., Lv, Z., Huo, Y. et al. (2019). A biodegradable functional water-responsive shape memory polymer for biomedical applications. *Journal of Materials Chemistry B* 7 (1): 123–132.
114 Zhu, Y., Hu, J., Luo, H. et al. (2012). Rapidly switchable water-sensitive shape-memory cellulose/elastomer nano-composites. *Soft Matter* 8 (8): 2509–2517.
115 Mishra, S.R. and Tracy, J.B. (2018). Sequential actuation of shape-memory polymers through wavelength-selective photothermal heating of gold nanospheres and nanorods. *ACS Applied Nano Materials* 1 (7): 3063–3067.
116 Han, D.-D., Zhang, Y.-L., Ma, J.-N. et al. (2016). Light-mediated manufacture and manipulation of actuators. *Advanced Materials* 28 (38): 8328–8343.
117 Liu, Y., Shaw, B., Dickey, M.D. et al. (2017). Sequential self-folding of polymer sheets. *Science Advances* 3 (3): e1602417.
118 Liu, Y., Boyles, J.K., Genzer, J. et al. (2012). Self-folding of polymer sheets using local light absorption. *Soft Matter* 8 (6): 1764–1769.
119 Vernon, L. and Vernon, H. (1941), *Producing molded articles such as dentures from thermoplastic synthetic resins*. US Patent 2234993.
120 Luo, X. and Mather, P.T. (2010). Conductive shape memory nanocomposites for high speed electrical actuation. *Soft Matter* 6 (10): 2146–2149.
121 Liu, R., Kuang, X., Deng, J. et al. (2018). Shape memory polymers for body motion energy harvesting and self-powered mechanosensing. *Advanced Materials* 30 (8): 1705195. -n/a.
122 Zarek, M., Layani, M., Cooperstein, I. et al. (2015). 3D printing of shape memory polymers for flexible electronic devices. *Advanced Materials* 28 (22): 4449–4454.
123 Zheng, N., Fang, G., Cao, Z. et al. (2015). High strain epoxy shape memory polymer. *Polymer Chemistry* 6 (16): 3046–3053.
124 Voit, W., Ware, T., Dasari, R.R. et al. (2010). High-strain shape-memory polymers. *Advanced Functional Materials* 20 (1): 162–171.

125 Yakacki, C.M., Shandas, R., Safranski, D. et al. (2008). Strong, tailored, biocompatible shape-memory polymer networks. *Advanced Functional Materials* 18 (16): 2428–2435.

126 Peng, B., Yang, Y., Gu, K. et al. (2019). Digital light processing 3D printing of triple shape memory polymer for sequential shape shifting. *ACS Materials Letters* 1 (4): 410–417.

127 Zotzmann, J., Behl, M., Feng, Y. et al. (2010). Copolymer networks based on poly(ω-pentadecalactone) and poly(ε-caprolactone)segments as a versatile triple-shape polymer system. *Advanced Functional Materials* 20 (20): 3583–3594.

128 Behl, M. and Lendlein, A. (2010). Triple-shape polymers. *Journal of Materials Chemistry* 20 (17): 3335–3345.

129 Xie, T. (2010). Tunable polymer multi-shape memory effect. *Nature* 464 (7286): 267–270.

130 Yu, K., Dunn, M.L., and Qi, H.J. (2015). Digital manufacture of shape changing components. *Extreme Mechanics Letters* 4: 9–17.

131 Kuang, X., Chen, K., Dunn, C.K. et al. (2018). 3D printing of highly stretchable, shape-memory and self-healing elastomer toward novel 4D printing. *ACS Applied Materials & Interfaces* 10 (8): 7381–7388.

132 Zhang, B., Zhang, W., Zhang, Z. et al. (2019). Self-healing four-dimensional printing with ultraviolet curable double network shape memory polymer system. *ACS Applied Materials & Interfaces* 11 (10): 10328–10336.

133 Yu, R., Yang, X., Zhang, Y. et al. (2017). Three-dimensional printing of shape memory composites with epoxy-acrylate hybrid photopolymer. *ACS Applied Materials & Interfaces* 9 (2): 1820–1829.

134 Kuang, X., Zhao, Z., Chen, K. et al. (2018). High-speed 3D printing of high-performance thermosetting polymers via two-stage curing. *Macromolecular Rapid Communications* 39 (7): 1700809.

135 Weigand, J.J., Miller, C.I., Janisse, A.P. et al. (2020). 3D printing of dual-cure benzoxazine networks. *Polymer* 189: 122193.

136 Han, B., Zhang, Y.L., Chen, Q.D. et al. (2018). Carbon-based photothermal actuators. *Advanced Functional Materials* 28 (40): 1802235.

137 Yang, H., Leow, W.R., Wang, T. et al. (2017). 3D printed photoresponsive devices based on shape memory composites. *Advanced Materials* 29 (33): 1701627.

138 Wang, Z., Tao, P., Liu, Y. et al. (2014). Rapid charging of thermal energy storage materials through plasmonic heating. *Scientific Reports* 4 (1): 1–8.

139 Tong, S., Quinto, C.A., Zhang, L. et al. (2017). Size-dependent heating of magnetic iron oxide nanoparticles. *ACS Nano* 11 (7): 6808–6816.

140 Fuhrer, R., Schumacher, C.M., Zeltner, M. et al. (2013). Soft iron/silicon composite tubes for magnetic peristaltic pumping: frequency-dependent pressure and volume flow. *Advanced Functional Materials* 23 (31): 3845–3849.

141 Razzaq, M., Behl, M., and Lendlein, A. (2012). Magnetic memory effect of nanocomposites. *Advanced Functional Materials* 22 (1): 184–191.

142 Kobayashi, K., Yoon, C., Oh, S.H. et al. (2018). Biodegradable thermomagnetically responsive soft untethered grippers. *ACS Applied Materials & Interfaces* 11 (1): 151–159.

143 He, Z., Satarkar, N., Xie, T. et al. (2011). Remote controlled multishape polymer nanocomposites with selective radiofrequency actuations. *Advanced Materials* 23 (28): 3192–3196.

144 Ze, Q., Kuang, X., Wu, S. et al. (2020). Magnetic shape memory polymers with integrated multifunctional shape manipulation. *Advanced Materials* 32 (4): 1906657.

145 Wei, H., Zhang, Q., Yao, Y. et al. (2017). Direct-write fabrication of 4D active shape-changing structures based on a shape memory polymer and its nanocomposite. *ACS Applied Materials & Interfaces* 9 (1): 876–883.

146 Hua, D., Zhang, X., Ji, Z. et al. (2018). 3D printing of shape changing composites for constructing flexible paper-based photothermal bilayer actuators. *Journal of Materials Chemistry C* 6 (8): 2123–2131.

147 Yuan, C., Wang, T., Dunn, M.L. et al. (2017). 3D printed active origami with complicated folding patterns. *International Journal of Precision Engineering and Manufacturing-Green Technology* 4 (3): 281–289.

148 Wu, J., Yuan, C., Ding, Z. et al. (2016). Multi-shape active composites by 3D printing of digital shape memory polymers. *Scientific Reports* 6: 24224.

149 Jeong, H.Y., Woo, B.H., Kim, N. et al. (2020). Multicolor 4D printing of shape-memory polymers for light-induced selective heating and remote actuation. *Scientific Reports* 10 (1): 6258.

150 Bodaghi, M., Damanpack, A., and Liao, W. (2016). Self-expanding/shrinking structures by 4D printing. *Smart Materials and Structures* 25 (10): 105034.

151 Teoh, J.E.M., An, J., Feng, X. et al. (2018). Design and 4D printing of cross-folded origami structures: a preliminary investigation. *Materials* 11 (3): 376.

152 van Manen, T., Janbaz, S., and Zadpoor, A.A. (2018). Programming the shape-shifting of flat soft matter. *Materials Today* 21 (2): 144–163.

153 Ding, Z., Yuan, C., Peng, X. et al. (2017). Direct 4D printing via active composite materials. *Science Advances* 3 (4): e1602890.

154 An, B., Y. Tao, J. Gu, et al. (2018). Thermorph: democratizing 4D printing of self-folding materials and interfaces. In *Proceedings of the 2018 CHI Conference on Human Factors in Computing Systems*. ACM.

155 Ding, Z., Weeger, O., Qi, H.J. et al. (2018). 4D rods: 3D structures via programmable 1D composite rods. *Materials & Design* 137: 256–265.

156 Yuan, C., Ding, Z., Wang, T. et al. (2017). Shape forming by thermal expansion mismatch and shape memory locking in polymer/elastomer laminates. *Smart Materials and Structures* 26 (10): 105027.

157 Zhang, Q., Zhang, K., and Hu, G. (2016). Smart three-dimensional lightweight structure triggered from a thin composite sheet via 3D printing technique. *Scientific Reports* 6: 22431.

158 Mao, Y., Yu, K., Isakov, M.S. et al. (2015). Sequential self-folding structures by 3D printed digital shape memory polymers. *Scientific Reports* 5: 13616.

159 Zhang, Q., Kuang, X., Weng, S. et al. (2021). Shape-memory balloon structures by pneumatic multi-material 4D printing. *Advanced Functional Materials* 2010872.

160 Liu, K., Wu, J., Paulino, G.H. et al. (2017). Programmable deployment of tensegrity structures by stimulus-responsive polymers. *Scientific Reports* 7 (1): 3511.

161 Wichterle, O. and Lim, D. (1960). Hydrophilic gels for biological use. *Nature* 185 (4706): 117–118.

162 Champeau, M., Heinze, D.A., Viana, T.N. et al. (2020). 4D printing of hydrogels: a review. *Advanced Functional Materials* 30 (31): 1910606.

163 Wu, Z.L., Moshe, M., Greener, J. et al. (2013). Three-dimensional shape transformations of hydrogel sheets induced by small-scale modulation of internal stresses. *Nature Communications* 4: 1586.

164 Kim, J., Hanna, J.A., Byun, M. et al. (2012). Designing responsive buckled surfaces by halftone gel lithography. *Science* 335 (6073): 1201–1205.

165 Han, D., Lu, Z., Chester, S.A. et al. (2018). Micro 3D printing of a temperature-responsive hydrogel using projection micro-stereolithography. *Scientific Reports* 8 (1): 1963.

166 Zhao, Z., Kuang, X., Yuan, C. et al. (2018). Hydrophilic/hydrophobic composite shape-shifting structures. *ACS Applied Materials & Interfaces* 10 (23): 19932–19939.

167 Zhao, Q., Yang, X., Ma, C. et al. (2016). A bioinspired reversible snapping hydrogel assembly. *Materials Horizons* 3 (5): 422–428.

168 Schild, H.G. (1992). Poly (N-isopropylacrylamide): experiment, theory and application. *Progress in Polymer Science* 17 (2): 163–249.

169 Illeperuma, W.R., Sun, J.-Y., Suo, Z. et al. (2013). Force and stroke of a hydrogel actuator. *Soft Matter* 9 (35): 8504–8511.

170 Bakarich, S.E., Gorkin, R., Panhuis, M.i.h. et al. (2015). 4D printing with mechanically robust, thermally actuating hydrogels. *Macromolecular Rapid Communications* 36 (12): 1211–1217.

171 Han, D., Farino, C., Yang, C. et al. (2018). Soft robotic manipulation and locomotion with a 3D printed electroactive hydrogel. *ACS Applied Materials & Interfaces* 10 (21): 17512–17518.

172 Jin, D., Chen, Q., Huang, T.-Y. et al. (2019). Four-dimensional direct laser writing of reconfigurable compound micromachines. *Materials Today* 32: 19–25.

173 Huang, T.-Y., Huang, H.-W., Jin, D.D. et al. (2020). Four-dimensional micro-building blocks. *Science Advances* 6 (3): eaav8219.

174 Sydney Gladman, A., Matsumoto, E.A., Nuzzo, R.G. et al. (2016). Biomimetic 4D printing. *Nature Materials* 15 (4): 413–418.

175 Kokkinis, D., Schaffner, M., and Studart, A.R. (2015). Multimaterial magnetically assisted 3D printing of composite materials. *Nature Communications* 6: 8643.

176 Mao, Y., Ding, Z., Yuan, C. et al. (2016). 3D printed reversible shape changing components with stimuli responsive materials. *Scientific Reports* 6: 24761.

177 Naficy, S., Gately, R., Gorkin, R. et al. (2017). 4D printing of reversible shape morphing hydrogel structures. *Macromolecular Materials and Engineering* 302 (1).

178 Liu, J., Erol, O., Pantula, A. et al. (2019). Dual-gel 4D printing of bioinspired tubes. *ACS Applied Materials & Interfaces* 11 (8): 8492–8498.

179 Huang, L., Jiang, R., Wu, J. et al. (2017). Ultrafast digital printing toward 4D shape changing materials. *Advanced Materials* 29 (7): 1605390. –n/a.

180 Kim, Y., Yeom, B., Arteaga, O. et al. (2016). Reconfigurable chiroptical nanocomposites with chirality transfer from the macro- to the nanoscale. *Nature Materials* 15 (4): 461–468.

181 Palagi, S., Mark, A.G., Reigh, S.Y. et al. (2016). Structured light enables biomimetic swimming and versatile locomotion of photoresponsive soft microrobots. *Nature Materials* 15 (6): 647–653.

182 Pei, Z., Yang, Y., Chen, Q. et al. (2014). Mouldable liquid-crystalline elastomer actuators with exchangeable covalent bonds. *Nature Materials* 13 (1): 36–41.

183 Yu, Y., Nakano, M., and Ikeda, T. (2003). Photomechanics: directed bending of a polymer film by light. *Nature* 425 (6954): 145–145.

184 Guin, T., Settle, M.J., Kowalski, B.A. et al. (2018). Layered liquid crystal elastomer actuators. *Nature Communications* 9 (1): 2531.

185 Wani, O.M., Zeng, H., and Priimagi, A. (2017). A light-driven artificial flytrap. *Nature Communications* 8: 15546.

186 Ware, T.H., McConney, M.E., Wie, J.J. et al. (2015). Voxelated liquid crystal elastomers. *Science* 347 (6225): 982–984.

187 Lu, X., Zhang, H., Fei, G. et al. (2018). Liquid-crystalline dynamic networks doped with gold nanorods showing enhanced photocontrol of actuation. *Advanced Materials* 30 (14): 1706597.

188 Kohlmeyer, R.R. and Chen, J. (2013). Wavelength-selective, IR light-driven hinges based on liquid crystalline elastomer composites. *Angewandte Chemie International Edition* 52 (35): 9234–9237.

189 Roach, D.J., Yuan, C., Kuang, X. et al. (2019). Long liquid crystal elastomer fibers with large reversible actuation strains for smart textiles and artificial muscles. *ACS Applied Materials & Interfaces* 11 (21): 19514–19521.

190 Saed, M.O., Torbati, A.H., Nair, D.P. et al. (2016). Synthesis of programmable main-chain liquid-crystalline elastomers using a two-stage thiol-acrylate reaction. *Journal of Visualized Experiments: JoVE* 0 (107): 53546.

191 Yakacki, C.M., Saed, M., Nair, D.P. et al. (2015). Tailorable and programmable liquid-crystalline elastomers using a two-stage thiol-acrylate reaction. *RSC Advances* 5 (25): 18997–19001.

192 Barnes, M. and Verduzco, R. (2019). Direct shape programming of liquid crystal elastomers. *Soft Matter* 15 (5): 870–879.

193 Li, Y., Zhang, Y., Rios, O. et al. (2017). Liquid crystalline epoxy networks with exchangeable disulfide bonds. *Soft Matter* 13 (29): 5021–5027.

194 Tabrizi, M., Ware, T.H., and Shankar, M.R. (2019). Voxelated molecular patterning in 3-dimensional Freeforms. *ACS Applied Materials & Interfaces* 11 (31): 28236–28245.

195 Kowalski, B.A., Guin, T.C., Auguste, A.D. et al. (2017). Pixelated polymers: directed self assembly of liquid crystalline polymer networks. *ACS Macro Letters* 6 (4): 436–441.

196 Ware, T.H., Perry, Z.P., Middleton, C.M. et al. (2015). Programmable liquid crystal elastomers prepared by thiol–ene photopolymerization. *ACS Macro Letters* 4 (9): 942–946.

197 Yu, L., Shahsavan, H., Rivers, G. et al. (2018). Programmable 3D shape changes in liquid crystal polymer networks of uniaxial orientation. *Advanced Functional Materials* 28 (37): 1802809.

198 Yuan, C., Roach, D.J., Dunn, C.K. et al. (2017). 3D printed reversible shape changing soft actuators assisted by liquid crystal elastomers. *Soft Matter* 13 (33): 5558–5568.

199 Zhao, R., Kim, Y., Chester, S.A. et al. (2019). Mechanics of hard-magnetic soft materials. *Journal of the Mechanics and Physics of Solids* 124: 244–263.

200 Hu, W., Lum, G.Z., Mastrangeli, M. et al. (2018). Small-scale soft-bodied robot with multimodal locomotion. *Nature* 554 (7690): 81.

201 Lum, G.Z., Ye, Z., Dong, X. et al. (2016). Shape-programmable magnetic soft matter. *Proceedings of the National Academy of Sciences of the United States of America* 113 (41): E6007–E6015.

202 Roh, S., Okello, L.B., Golbasi, N. et al. (2019). 3D-printed silicone soft architectures with programmed magneto-capillary reconfiguration. *Advanced Materials Technologies* 4 (4): 1800528.

203 Cui, J., Huang, T.-Y., Luo, Z. et al. (2019). Nanomagnetic encoding of shape-morphing micromachines. *Nature* 575 (7781): 164–168.

204 Rahmer, J., Stehning, C., and Gleich, B. (2017). Spatially selective remote magnetic actuation of identical helical micromachines. *Science Robotics* 2 (3): eaal2845.

205 Kim, Y., Parada, G.A., Liu, S. et al. (2019). Ferromagnetic soft continuum robots. *Science Robotics* 4 (33): eaax7329.

206 Wu, S., Ze, Q., Zhang, R. et al. (2019). Symmetry-breaking actuation mechanism for soft robotics and active metamaterials. *ACS Applied Materials & Interfaces* 11 (44): 41649–41658.

207 Montgomery, S.M., Wu, S., Kuang, X. et al. (2020). Magneto-mechanical metamaterials with widely Tunable mechanical properties and acoustic bandgaps. *Advanced Functional Materials* n/a(n/a): 2005319.

208 Kim, J., Chung, S.E., Choi, S.-E. et al. (2011). Programming magnetic anisotropy in polymeric microactuators. *Nature Materials* 10 (10): 747.

209 Xu, T., Zhang, J., Salehizadeh, M. et al. (2019). Millimeter-scale flexible robots with programmable three-dimensional magnetization and motions. *Science Robotics* 4 (29): eaav4494.

210 Peters, C., Hoop, M., Pané, S. et al. (2016). Degradable magnetic composites for minimally invasive interventions: device fabrication, targeted drug delivery, and cytotoxicity tests. *Advanced Materials* 28 (3): 533–538.

211 Lee, Y.-W., Ceylan, H., Yasa, I.C. et al. (2021). 3D-printed multi-stimuli-responsive mobile micromachines. *ACS Applied Materials & Interfaces* 13 (11): 12759–12766.

212 Ji, Z., Yan, C., Yu, B. et al. (2017). Multimaterials 3D printing for free assembly manufacturing of magnetic driving soft actuator. *Advanced Materials Interfaces* 4 (22): 1700629.

213 van Rees, W.M., Vouga, E., and Mahadevan, L. (2017). Growth patterns for shape-shifting elastic bilayers. *Proceedings of the National Academy of Sciences of the United States of America* 114 (44): 11597–11602.

214 Sossou, G., Demoly, F., Belkebir, H. et al. (2019). Design for 4D printing: a voxel-based modeling and simulation of smart materials. *Materials & Design* 175: 107798.

215 Westbrook, K.K., Parakh, V., Chung, T. et al. (2010). Constitutive modeling of shape memory effects in semicrystalline polymers with stretch induced crystallization. *Journal of Engineering Materials and Technology* 132 (4): 041010-041010-9.

216 Ge, Q., Luo, X., Rodriguez, E.D. et al. (2012). Thermomechanical behavior of shape memory elastomeric composites. *Journal of the Mechanics and Physics of Solids* 60 (1): 67–83.

217 Ge, Q., Luo, X., Iversen, C.B. et al. (2014). A finite deformation thermomechanical constitutive model for triple shape polymeric composites based on dual thermal transitions. *International Journal of Solids and Structures* 51 (15): 2777–2790.

218 Mao, Y., Chen, F., Hou, S. et al. (2019). A viscoelastic model for hydrothermally activated malleable covalent network polymer and its application in shape memory analysis. *Journal of the Mechanics and Physics of Solids* 127: 239–265.

219 Hamel, C.M., Cui, F., and Chester, S.A. (2017). A finite element method for light activated shape-memory polymers. *International Journal for Numerical Methods in Engineering* 111 (5): 447–473.

220 Warner, M. and Terentjev, E.M. (2003). *Liquid Crystal Elastomers*, vol. 120. OUP Oxford.

221 Oates, W. and Wang, H. (2009). A new approach to modeling liquid crystal elastomers using phase field methods. *Modelling and Simulation in Materials Science and Engineering* 17 (6): 064004.

222 Zhang, Y., Xuan, C., Jiang, Y. et al. (2019). Continuum mechanical modeling of liquid crystal elastomers as dissipative ordered solids. *Journal of the Mechanics and Physics of Solids* 126: 285–303.

223 Chester, S.A., Di Leo, C.V., and Anand, L. (2015). A finite element implementation of a coupled diffusion-deformation theory for elastomeric gels. *International Journal of Solids and Structures* 52 (Supplement C): 1–18.

224 Zhao, Z., Wu, J., Mu, X. et al. (2017). Desolvation induced origami of photocurable polymers by digit light processing. *Macromolecular Rapid Communications* 38 (13): 1600625. -n/a.

225 Bosnjak, N., Wang, S., Han, D. et al. (2019). Modeling of fiber-reinforced polymeric gels. *Mechanics Research Communications* 96: 7–18.

226 Craig, H., Devin, R., Kevin, L. et al. (2019). Machine-learning based design of active composite structures for 4D printing. *Smart Materials and Structures* 28: 065005.

227 Geiss, M., Boddeti, N., Weeger, O. et al. (2018). Combined level-set-XFEM-density topology optimization of 4D printed structures undergoing large deformation. *Journal of Mechanical Design* 141.

228 Sossou, G., Demoly, F., Belkebir, H. et al. (2019). Design for 4D printing: modeling and computation of smart materials distributions. *Materials & Design* 181: 108074.

229 Sigmund, O. (2001). Design of multiphysics actuators using topology optimization – part I: one-material structures. *Computer Methods in Applied Mechanics and Engineering* 190 (49): 6577–6604.

230 Sigmund, O. (2001). Design of multiphysics actuators using topology optimization – part II: two-material structures. *Computer Methods in Applied Mechanics and Engineering* 190 (49): 6605–6627.

231 Maute, K., Tkachuk, A., Wu, J. et al. (2015). Level set topology optimization of printed active composites. *Journal of Mechanical Design* 137 (11): 111402.

232 Kuang, X., Wu, S., Ze, Q. et al. (2021). Magnetic dynamic polymers for modular assembling and reconfigurable morphing architectures. *Advanced Materials* 33 (30): e2102113.

233 Montarnal, D., Capelot, M., Tournilhac, F. et al. (2011). Silica-like malleable materials from permanent organic networks. *Science* 334 (6058): 965–968.

234 Podgórski, M., Fairbanks, B.D., Kirkpatrick, B.E. et al. Toward stimuli-responsive dynamic thermosets through continuous development and improvements in covalent adaptable networks (CANs). *Advanced Materials*. **n/a**(n/a) 1906876.

235 Chakma, P. and Konkolewicz, D. (2019). Dynamic covalent bonds in polymeric materials. *Angewandte Chemie International Edition*.

236 Denissen, W., Winne, J.M., and Du Prez, F.E. (2016). Vitrimers: permanent organic networks with glass-like fluidity. *Chemical Science* 7 (1): 30–38.

237 Deng, J., Kuang, X., Liu, R. et al. (2018). Vitrimer elastomer-based jigsaw puzzle-like healable triboelectric nanogenerator for self-powered wearable electronics. *Advanced Materials* 30 (14): 1705918. -n/a.

238 Denissen, W., Droesbeke, M., Nicolaÿ, R. et al. (2017). Chemical control of the viscoelastic properties of vinylogous urethane vitrimers. *Nature Communications* 8 (1): 14857.

239 Rekondo, A., Martin, R., de Luzuriaga, A.R. et al. (2014). Catalyst-free room-temperature self-healing elastomers based on aromatic disulfide metathesis. *Materials Horizons* 1 (2): 237–240.

240 Davidson, E.C., Kotikian, A., Li, S. et al. (2019). 3D printable and reconfigurable liquid crystal elastomers with light-induced shape memory via dynamic bond exchange. *Advanced Materials* 32 (1): e1905682.

241 Zhang, G., Peng, W., Wu, J. et al. (2018). Digital coding of mechanical stress in a dynamic covalent shape memory polymer network. *Nature Communications* 9 (1): 4002.

242 Yang, Y., Chen, Z., Song, X. et al. (2017). Biomimetic anisotropic reinforcement architectures by electrically assisted nanocomposite 3D printing. *Advanced Materials* 29 (11): 1605750. –n/a.

243 Yang, Y., Xuan, S., Xiangjia, L. et al. (2018. **0**(0)). Recent Progress in biomimetic additive manufacturing technology: from materials to functional structures. *Advanced Materials* 1706539.

244 Studart, A.R. (2016). Additive manufacturing of biologically-inspired materials. *Chemical Society Reviews* 45 (2): 359–376.

245 Regehly, M., Garmshausen, Y., Reuter, M. et al. (2020). Xolography for linear volumetric 3D printing. *Nature* 588 (7839): 620–624.

246 Kelly, B.E., Bhattacharya, I., Heidari, H. et al. (2019). Volumetric additive manufacturing via tomographic reconstruction. *Science* 363 (6431): eaau7114.

247 de Beer, M.P., van der Laan, H.L., Cole, M.A. et al. (2019). Rapid, continuous additive manufacturing by volumetric polymerization inhibition patterning. *Science Advances* 5 (1): eaau8723.

248 Shusteff, M., Browar, A.E., Kelly, B.E. et al. (2017). One-step volumetric additive manufacturing of complex polymer structures. *Science Advances* 3 (12): eaao5496.

249 Walker, D.A., Hedrick, J.L., and Mirkin, C.A. (2019). Rapid, large-volume, thermally controlled 3D printing using a mobile liquid interface. *Science* 366 (6463): 360–364.

250 Erb, R.M., Sander, J.S., Grisch, R. et al. (2013). Self-shaping composites with programmable bioinspired microstructures. *Nature Communications* 4: 1712.

251 Martin, J.J., Fiore, B.E., and Erb, R.M. (2015). Designing bioinspired composite reinforcement architectures via 3D magnetic printing. *Nature Communications* 6: 8641.